

# Refining the mass estimate for the intermediate-mass black hole candidate in NGC 3319

Benjamin L. Davis<sup>1,2,\*</sup>  and Alister W. Graham<sup>1</sup> 

<sup>1</sup>Centre for Astrophysics and Supercomputing, Swinburne University of Technology, Hawthorn, VIC 3122, Australia

<sup>2</sup>Center for Astro, Particle, and Planetary Physics (CAP<sup>3</sup>), New York University Abu Dhabi

## Abstract

Recent X-ray observations by Jiang et al. have identified an active galactic nucleus (AGN) in the bulgeless spiral galaxy NGC 3319, located just  $14.3 \pm 1.1$  Mpc away, and suggest the presence of an intermediate-mass black hole (IMBH;  $10^2 \leq M_{\bullet}/M_{\odot} \leq 10^5$ ) if the Eddington ratios are as high as 3 to  $3 \times 10^{-3}$ . In an effort to refine the black hole mass for this (currently) rare class of object, we have explored multiple black hole mass scaling relations, such as those involving the (not previously used) velocity dispersion, logarithmic spiral-arm pitch angle, total galaxy stellar mass, nuclear star cluster mass, rotational velocity, and colour of NGC 3319, to obtain ten mass estimates, of differing accuracy. We have calculated a mass of  $3.14_{-2.20}^{+7.02} \times 10^4 M_{\odot}$ , with a confidence of 84% that it is  $\leq 10^5 M_{\odot}$ , based on the combined probability density function from seven of these individual estimates. Our conservative approach excluded two black hole mass estimates (via the nuclear star cluster mass, and the fundamental plane of black hole activity — which only applies to black holes with low accretion rates) that were upper limits of  $\sim 10^5 M_{\odot}$ , and it did not use the  $M_{\bullet}-L_{2-10 \text{ keV}}$  relation's prediction of  $\sim 10^5 M_{\odot}$ . This target provides an exceptional opportunity to study an IMBH in AGN mode and advance our demographic knowledge of black holes. Furthermore, we introduce our novel method of meta-analysis as a beneficial technique for identifying new IMBH candidates by quantifying the probability that a galaxy possesses an IMBH.

**Keywords:** black hole physics – galaxies: active – galaxies: evolution – galaxies: individual: NGC 3319 – galaxies: spiral – galaxies: structure

Original unedited manuscript, accepted for publication by PASA, May 7, 2021.

## 1 INTRODUCTION

There is a largely-missing population of intermediate-mass black holes (IMBHs) with masses higher than those formed by stable, single stars today ( $M_{\bullet} \lesssim 100 M_{\odot}$ ) and less massive than the supermassive black holes (SMBHs;  $10^5 M_{\odot} \leq M_{\bullet} \lesssim 10^{10} M_{\odot}$ )<sup>1</sup> known to reside at the centres of massive galaxies. Not surprisingly, astronomers around the world have been hotly pursuing the much-anticipated discovery of IMBHs for some time (e.g. Miller & Colbert, 2004). In addition to providing a fundamental input to the cosmic inventory of our Universe, the abundance, or rarity, of IMBHs has implications for the formation of the Universe's SMBHs (Graham, 2016b;

Mezcua, 2017; Koliopanos, 2017; Inayoshi et al., 2020; Sahu et al., 2019a).

As yet, there is no consensus as to how SMBHs came to be. While the observed extent of quasar activity over the history of our Universe has revealed that the accretion of baryons fattened them up (e.g. Soltan, 1982; Shankar et al., 2004), we do not know what their (potentially range of) birth masses were. Some theories have speculated that their birth or 'seed' masses were  $\approx 10^5 M_{\odot}$ , thereby providing a kick-start to explain the early-formation of the high- $z$ , active galactic nuclei (AGN) with sizeable black hole masses around  $\approx 10^9 M_{\odot}$  (e.g. Mortlock et al., 2011; Yang et al., 2020; Mignoli et al., 2020). Theories have included primordial black holes (e.g. Grobov et al., 2011), massive metal-free Population III stars which subsequently collapse (or collide, e.g. Alister Seguel et al., 2020) to form massive black holes (e.g. Madau & Rees, 2001; Schneider et al., 2002),

\* Author for correspondence: BLD, E-mail: ben.davis@nyu.edu

<sup>1</sup>The massive central object in the quasar TON 618 is alleged to have the most massive black hole with a mass of  $6.61 \times 10^{10} M_{\odot}$ , estimated from its H $\beta$  emission line and a virial  $f$ -factor of 5.5 (Shemmer et al., 2004; Onken et al., 2004).

or the direct collapse of massive gas clouds, effectively by-passing the stellar phase of evolution (e.g. Bromm & Loeb, 2003; Mayer et al., 2010).

The suggestion of massive seeds arose from the notion that the ‘Eddington limit’ (Eddington, 1925) of gas accretion onto a black hole implied that stellar-mass black holes did not have sufficient time to grow into the SMBHs observed in the young, high-redshift AGN. However, the Eddington limit on the accretion rate applies only to (unrealistic) spherical conditions (Nayakshin et al., 2012; Alexander & Natarajan, 2014) and can be significantly exceeded in real systems. For example, super-critical (super-Eddington) accretion flows onto massive black holes can occur when the accretion flow is mostly confined to the disk plane while most of the radiation emerges in outflows along the rotation axis (Abramowicz et al., 1980; Jiang et al., 2014; Pezzulli et al., 2016). Hyper-Eddington accretion rates can exist in spherically-symmetric accretion flows when energy advection reduces radiative efficiency (Inayoshi et al., 2016). Thus, the practicality of super-critical accretion has been invoked to explain the early existence of SMBHs at high redshifts (Volonteri & Rees, 2005; Volonteri, 2012; Volonteri & Bellovary, 2012; Volonteri et al., 2015). Besides, most ultra-luminous X-ray sources are nowadays explained as stellar-mass X-ray binaries accreting much faster than their Eddington limit (Feng & Soria, 2011; Kaaret et al., 2017). Such accretion negates the need for massive black hole seeds.

An additional motive for starting AGN with massive seeds was that black holes with masses intermediate between that of stellar-mass black holes and SMBHs had not been directly observed, and therefore seemed not to exist. However, this may be a sample selection bias because the sphere-of-gravitational-influence around such IMBHs, where one would directly observe a Keplerian rotation curve, is typically too small to resolve spatially. Furthermore, there is now a rapidly rising number of IMBH candidates based upon indirect estimates of the black hole mass (Farrell et al., 2009; Secrest et al., 2012; Baldassare et al., 2015; Graham et al., 2016; Kızıltan et al., 2017; Nguyen et al., 2017; Chilingarian et al., 2018; Mezcuca et al., 2018; Jiang et al., 2018; Nguyen et al., 2019; Graham & Soria, 2019; Graham et al., 2019; Woo et al., 2019; Lin et al., 2020). In addition, there are currently five IMBH candidates in the Milky Way (Takekawa et al., 2020).

There is no shortage of scenarios for how a bridging population of IMBHs may have arisen. Possible pathways include the runaway collapse of dense ‘nuclear star clusters’ (Portegies Zwart & McMillan, 2002; Davies et al., 2011; Lupi et al., 2014; Stone et al., 2017), especially if gas-drag and dynamical friction are in play at the centre of a galaxy, or the gas-fuelled growth of a stellar-mass black hole that has not yet devoured enough material to become an SMBH (Natarajan, 2021). These

ideas would place, at least some, IMBHs at the centres of galaxies, where established black hole mass scaling relations involving some property of the host galaxy can be applied.

Recent *Chandra X-ray Observatory* (CXO; Weisskopf et al., 2000) observations (Soria, 2016, see also Chilingarian et al. 2018 and Bi et al. 2020), have discovered IMBH candidates at the centres<sup>2</sup> of several nearby, low-mass galaxies. Long exposures have enabled the discovery of faint X-ray point-sources (consistent with low-mass black holes accreting with low Eddington ratios) in galaxies which have been predicted to host a central IMBH based upon each galaxy’s velocity dispersion, luminosity, and spiral-arm pitch angle (Koliopanos et al., 2017; Graham & Soria, 2019; Graham et al., 2019). The high-energy X-ray photons, originating from the (not so) dead centres of the galaxies, are likely coming from the accretion disks around black holes because of their point-source nature, where emission favours active black holes rather than spatially extended star formation.

Several studies have identified IMBH candidates in galaxies based on single, or a few, black hole mass estimates. In this work, we have selected a galaxy, NGC 3319, where we can apply a wealth of independent black hole mass estimates. NGC 3319 is a gas-rich, bulgeless, late-type galaxy. It is a strongly-barred spiral galaxy classified as SBcd(rs) (de Vaucouleurs et al., 1991) and has its bar aligned with the major axis (Randriamampandry et al., 2015). Moreover, Jiang et al. (2018) identify it as possessing a low-luminosity AGN with a high-accretion-rate signalled by a nuclear X-ray point source and assume a black hole mass between  $3 \times 10^2 M_{\odot}$  and  $3 \times 10^5 M_{\odot}$  based on a high Eddington ratio of 1 to  $10^{-3}$ , despite a non-detection in the radio. Using the X-ray variability, they report an estimate of  $\sim 10^{5 \pm 2} M_{\odot}$ , and using the ‘fundamental plane of black hole activity’, they reported an upper limit of  $10^5 M_{\odot}$  in the absence of radio data. NGC 3319 had previously been recognised as a possible low-ionisation nuclear emission-line region (LINER) galaxy (Heckman et al., 1980; Pogge, 1989), or at least it possessed an uncertain H II nucleus (Ho et al., 1997). Recently, Baldi et al. (2018) classified its nuclear type as a LINER based on BPT (Baldwin et al., 1981) diagram diagnostics. This classification is of significance since AGN with black holes are suspected sources of stimulating LINER spectral emission (Heckman, 1980).

In this study, we endeavour to constrain better the mass of the potential IMBH in the nucleus of NGC 3319

<sup>2</sup>Some of the off-centre X-ray sources that were detected may also be IMBHs. Indeed, the best localised IMBH candidate to date is an off-centre source in the galaxy ESO 243-49 (Farrell et al., 2009), whose optical counterpart was discovered by Soria et al. (2010) and is thought to be the nucleus of an in-falling galaxy. However, the likelihoods of these off-centre targets being IMBHs are generally considered to be notably lower than that of the central targets — although perhaps not zero (e.g. Barrows et al., 2019; Bellovary et al., 2021).

via a meta-analysis of multiple mass estimates based on independently measured quantities. In the numerous subsections of Section 2, we present a detailed analysis and application of ten separate black hole mass scaling relations and ultimately combine these estimates to yield an overall black hole mass estimate with confidence limits. The uncertainty on each mass estimate is used to weight every estimate before combining the results, via standard statistical techniques, to obtain the final mass estimate whose uncertainty is naturally less than that of the individual mass estimates. In the final section (Section 3), we discuss the results of our investigation, comment on the implications, and remark on the benefit from continued study of NGC 3319.

Following Jiang et al. (2018), we adopt a redshift-independent luminosity distance of  $14.3 \pm 1.1$  Mpc (Cepheid variable star distance from Sakai et al., 1999), with a physical scale of  $69 \pm 5$  pc arcsec<sup>-1</sup>. All values from the literature have been adjusted to accommodate our adopted distance to NGC 3319. Black hole masses ( $M_{\bullet}$ ) and other masses throughout this work are represented as logarithmic (solar) mass values, i.e.  $\mathcal{M} \equiv \log M$ , where  $M$  is mass in units of solar masses ( $M_{\odot}$ ). All uncertainties are presented as (or have been scaled to)  $1\sigma \approx 68.3\%$  confidence intervals. All magnitudes are given in the AB system (Oke, 1974).

## 2 BLACK HOLE MASS ESTIMATES

In the following subsections (2.1–2.10), we applied ten different black hole mass scaling relations to estimate the mass of the black hole (NGC 3319\*) residing at the centre of NGC 3319. We use the latest, and thus in some instances morphology-dependent, black hole scaling relations. Although the use of reverberation mapping has revealed that AGN extend the  $M_{\bullet}$ – $M_{\text{bulge},*}$  relation to black hole masses of  $10^5 M_{\odot}$  (Graham & Scott, 2015), the paucity of confirmed IMBHs (and thus their dearth in the construction of black hole mass scaling relations) requires us to extrapolate these relations to reach into the IMBH regime.<sup>3</sup> Albeit, we note that NGC 205 (Nguyen et al., 2019) and NGC 404 (Nguyen et al., 2017) now extend the relations down to  $\sim 10^4$  and  $\sim 10^5 M_{\odot}$ , respectively. In Section 2.11, we combine the black hole mass estimates, accounting for the different levels of scatter in each estimate.

### 2.1 The $M_{\bullet}$ – $\phi$ relation

The aesthetic beauty of ‘spiral nebulae’ has been observed for 175 years, since Lord Rosse’s observations of the Whirlpool Galaxy (NGC 5194). However, significant mysteries still abound between the nature of

these striking features and properties of their host galaxies (D’Onghia et al., 2013). The seminal works that established the spiral density wave theory (Lin & Shu, 1964, 1966; Lin et al., 1969) have provided perhaps the most lucid and lasting explanation of (grand design) spiral genesis. Indeed, the spiral density theory has been supported by observations in numerous studies (Davis et al., 2015; Pour-Imani et al., 2016; Yu & Ho, 2018; Peterken et al., 2019; Miller et al., 2019; Vallée, 2019, 2020; Abdeen et al., 2020; Griv et al., 2020, 2021).

In particular, Lin & Shu (1966) predicted that the geometry of spiral patterns should be governed by two primary galactic properties: (i) the density of the galactic disk and (ii) the central gravitational potential (mass) of the galaxy. Specifically, the pitch angle of the spiral pattern at a distance  $R$  from a galaxy’s centre should be directly proportional to the density of the disk at  $R$  and inversely proportional to the mass of the galaxy  $\leq R$ . Davis et al. (2015) tested this prediction and found a tight trivariate relationship between the pitch angle, the stellar bulge mass, and the neutral atomic hydrogen density in the disk of a galaxy. Additional studies pertaining to dark matter halos have also shown a correlation between pitch angle and the central mass concentration, as determined by the shear of the rotation curve of a galaxy (Seigar et al., 2006, 2014). These theoretical and observational studies provide perhaps the best explanations of why the pitch angle correlates with its host galaxy: the pitch angle is clearly related to the central mass of a galaxy, of which the ‘barge’ (bar and bulge) and black hole are integral components entwined via coevolution.

The geometry of logarithmic spirals closely matches the shape of spiral arms in galaxies. Quantitatively, the shape (tightness of winding) of a logarithmic spiral is governed by the absolute value of its pitch angle,<sup>4</sup>  $|\phi|$ , as introduced by von der Pahlen (1911). Seigar et al. (2008) first presented evidence of a strong relationship between pitch angle and the mass of a spiral galaxy’s central black hole. As the sample of spiral galaxies with directly-measured black hole masses grew incrementally in size over the years, Berrier et al. (2013) and later Davis et al. (2017) presented refinements to the  $M_{\bullet}$ – $\phi$  relation. A graphical representation of the relation found by Davis et al. (2017, equation 8) is shown in Fig. 1. We employ equation 8 from Davis et al. (2017) to convert measured pitch angles into black hole masses, including an intrinsic scatter of 0.33 dex (added in quadrature with a full propagation of errors on the pitch angle measurement, as well as errors on the slope and intercept of the relation).

The existence of an  $M_{\bullet}$ – $\phi$  relation has been seen not only in observations (Seigar et al., 2008; Berrier et al.,

<sup>3</sup>This is also the case with reverberation mapping, which assumes the  $f$ -factor (used to convert virial products into virial masses) holds constant.

<sup>4</sup>For introductory reading on pitch angle, see section 2 from Davis et al. (2017).

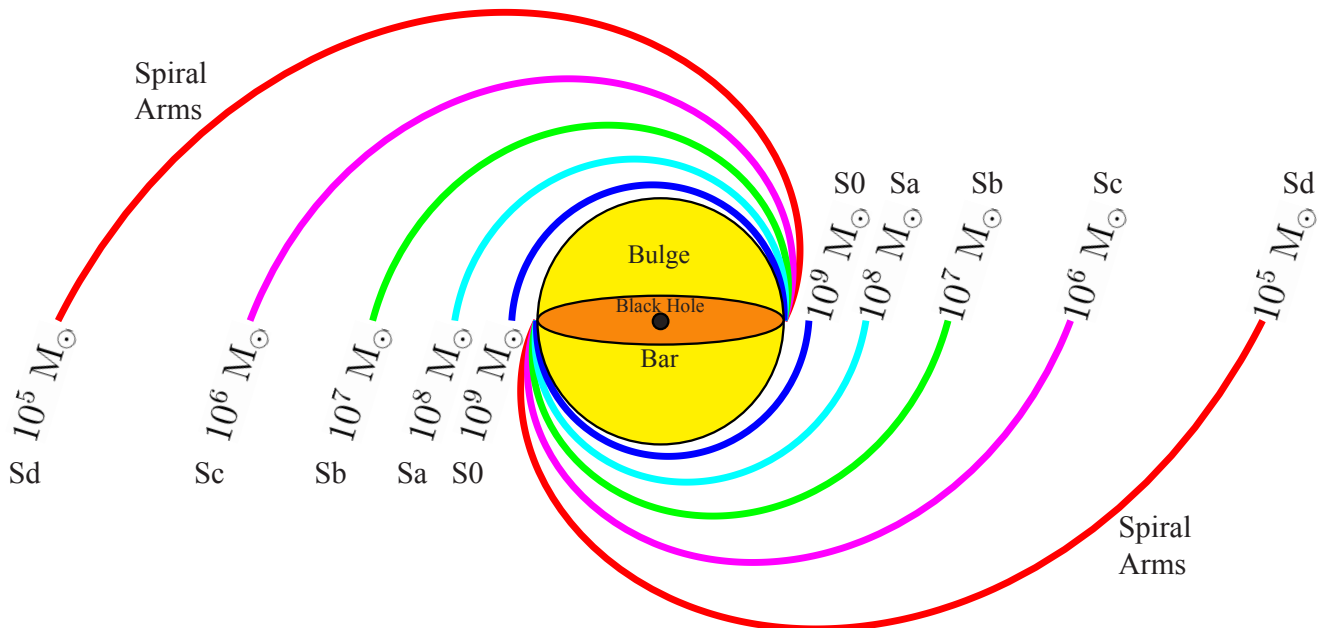


**Figure 1.** Spiral galaxy arms with varying degrees of tightness, with the corresponding galaxy morphological type and central black hole mass in units of our Sun’s mass. This template can be used to estimate central black hole masses in spiral galaxies. The outermost spiral (—) has  $|\phi| = 26^\circ.7$ , which is indicative of a central black hole with a mass of  $10^5 M_\odot$  via equation 8 from Davis et al. (2017).

2013; Davis et al., 2017) but also in simulations. Mutlu-Pakdil et al. (2018) measured the pitch angles for a random sample of 95 galaxies drawn from the *Illustris* simulation (Vogelsberger et al., 2014) and recovered an  $M_\bullet$ - $\phi$  relation that was consistent with that found from observational studies. Thus, the nascent  $M_\bullet$ - $\phi$  relation has already garnered empirical and theoretical (via theory and simulations) support to become a full-fledged black hole mass scaling relation. Its progress has proliferated in only a dozen years; future improvements in observations and sample size should add to its established legitimacy. The search for the primary relation with black hole mass continues, and the lack of a spiral pattern in early-type galaxies rules out the  $M_\bullet$ - $\phi$  relation, just as the absence of bulges in some late-type galaxies negates the  $M_\bullet$ - $M_{\text{bulge},*}$  relation. Nonetheless, the low level of scatter in both relations make them valuable black hole mass estimators.

Several software programs have been devised to handle the quantitative measurement of spiral galaxy pitch angle. In this work, we utilise three of the most prominent and robust packages to measure pitch angle: 2DFFT (Davis et al., 2012, 2016; Seigar et al., 2018), SPIRALITY (Shields et al., 2015a,b), and SPARCFIRE (Davis & Hayes, 2014). Each code uses an independent method of measuring pitch angle, each with its unique advantage.<sup>5</sup> Each routine measures pitch angle after

the original galaxy image (Fig. 2, left panel) has been deprojected to an artificial *face-on* orientation (Fig. 2, middle panel). We adopt the outer isophote position angle ( $PA_{\text{outer}}$ , degrees east of north) and ellipticity ( $\epsilon_{\text{outer}}$ ) values for NGC 3319 from Salo et al. (2015):  $PA_{\text{outer}} = 43^\circ.0 \pm 0^\circ.7$  and  $\epsilon_{\text{outer}} = 0.435 \pm 0.003$ . This ellipticity is equivalent to an inclination of the disk,  $i_{\text{disk}} \equiv \cos^{-1}(1 - \epsilon_{\text{outer}}) = 55^\circ.6 \pm 0^\circ.2$ .

We measured the pitch angles from a *Spitzer Space Telescope* Infrared Array Camera (IRAC)  $8.0 \mu\text{m}$  image obtained from the *Spitzer Heritage Archive*.<sup>6</sup> Recent studies (Pour-Imani et al., 2016; Miller et al., 2019) have presented observational evidence that  $8.0\text{-}\mu\text{m}$  light highlights the physical location of the spiral density wave in spiral galaxies.  $8.0\text{-}\mu\text{m}$  light comes from the glow of warm dust around nascent natal star-forming regions that have been shocked into existence by the spiral density wave.

### 2.1.1 SPARCFIRE

SPARCFIRE (Davis & Hayes, 2014) uses computer vision techniques to identify the pixel clusters that form the architecture of spiral arms in spiral galaxies and fits logarithmic spiral segments to the clusters. SPARCFIRE classifies each spiral based on its chirality: Z-wise, spirals that grow radially in a counterclockwise direction ( $\phi < 0$ ); and S-wise, spirals that grow radially in

<sup>5</sup>For a demonstrative comparison of each software package, see the appendix from Davis et al. (2017).

<sup>6</sup><https://irsa.ipac.caltech.edu/applications/Spitzer/SHA>

a clockwise direction ( $\phi > 0$ ). Based on the number and arc lengths of the ensemble of fitted spirals, we adopted a dominant chirality for the galaxy and ignored all spurious arcs matching the secondary chirality. We calculated a weighted-arithmetic-mean pitch angle for the galaxy based on a weight for each arc ( $w_i$ ) such that  $w_i \equiv s_i/r_{0,i}$ , where  $s_i$  is the arc length and  $r_{0,i}$  is the inner radius (from the origin at the galactic centre) for an individual arc segment. Therefore, the highest weighting resides with long arcs near the centre of the galaxy and short, possibly spurious arc segments in the outer region of the galaxy, are made insignificant.

As seen in the right panel of Fig. 2, the dominant chirality is Z-wise. We computed the pitch angle and converted it to a black hole mass prediction via the  $M_{\bullet}$ - $\phi$  relation as follows,

$$\begin{aligned} |\phi|_{\text{SPARCFIRE}} &= 31.7 \pm 4.5 \rightarrow \\ \mathcal{M}_{\bullet}(|\phi|_{\text{SPARCFIRE}}) &= 4.15 \pm 0.86. \end{aligned} \quad (1)$$

### 2.1.2 2DFFT

2DFFT (Davis et al., 2012, 2016; Seigar et al., 2018) is a two-dimensional fast *Fourier* transform software package that decomposes a galaxy image into logarithmic spirals. It computes the amplitude of each *Fourier* component by decomposing the observed distribution of light in an image into a superposition of logarithmic spirals as a function of pitch angle,  $\phi$ , and harmonic-mode,  $m$ , i.e. the order of rotational symmetry (e.g. two-fold, three-fold, and higher-order symmetries). For the *face-on* view of NGC 3319 (Fig. 2, middle panel), the maximum amplitude is achieved with  $m = 2$  (i.e. two spiral arms) and

$$|\phi|_{2\text{DFFT}} = 28.4 \pm 3.5 \rightarrow \mathcal{M}_{\bullet}(|\phi|_{2\text{DFFT}}) = 4.72 \pm 0.70. \quad (2)$$

### 2.1.3 SPIRALITY

SPIRALITY (Shields et al., 2015a,b) is a template-fitting software. Given a *face-on* image of a spiral galaxy, it computes a library of spiral coordinate systems with varying pitch angles. For NGC 3319 (Fig. 2, middle panel), the best-fitting spiral coordinate system has a pitch angle of

$$\begin{aligned} |\phi|_{\text{SPIRALITY}} &= 24.4 \pm 4.1 \rightarrow \\ \mathcal{M}_{\bullet}(|\phi|_{\text{SPIRALITY}}) &= 5.40 \pm 0.74. \end{aligned} \quad (3)$$

### 2.1.4 Weighted-mean pitch angle and black hole mass

The  $M_{\bullet}$ - $\phi$  relation is a tight relation, with intrinsically low scatter. However, the slope of the relation is relatively steep, and thus small changes in pitch angle equate to large changes in black hole mass. Specifically, a change in pitch angle of only 5.8 is associated with a 1.0 dex change in black hole mass. For late-type spiral galaxies like NGC 3319, their open spiral structures often

feature inherent flocculence and asymmetries amongst individual spiral arms. Furthermore, due to the diminished total masses of these galaxies (as compared to early-type spiral galaxies), galaxy harassment and tidal interactions are more impactful in disrupting their spiral structures.

The average uncertainty amongst our equations 1–3 is 4.0 (a difference of 0.68 dex in black hole mass). Nonetheless, all three of the pitch angle measurements possess overlapping error bars. To produce a more robust pitch angle measurement, we combine all three measurements (equations 1–3) to yield a weighted-arithmetic-mean pitch angle,

$$\bar{\phi} = \frac{\sum_{i=1}^N w_i \phi_i}{\sum_{i=1}^N w_i}, \quad (4)$$

and associated uncertainty,

$$\delta\bar{\phi} = \frac{\sqrt{\sum_{i=1}^N (w_i \delta\phi_i)^2}}{\sum_{i=1}^N w_i} = \sqrt{\frac{1}{\sum_{i=1}^N w_i}}, \quad (5)$$

with a weight for each measurement that is inversely proportional to the square of the uncertainty of its measurement, i.e. inverse-variance weighting,  $w_i = (\delta\phi_i)^{-2}$ . This yields

$$|\bar{\phi}| = 28.0 \pm 2.3 \rightarrow \mathcal{M}_{\bullet}(|\bar{\phi}|) = 4.79 \pm 0.54. \quad (6)$$

Our use of the independent black hole mass scaling relations, and their reported  $\pm 1\sigma$  scatter, assumes a normal distribution for each. Assuming a normal distribution for our weighted-mean, we can then calculate the probability of having an IMBH. Given a mass estimate for a black hole and its associated error ( $\delta\mathcal{M}_{\bullet}$ ), we can compute the probability that the black hole is less-than-supermassive ( $\mathcal{M}_{\bullet} \leq 5$ ) as follows,

$$P(\mathcal{M}_{\bullet} \leq 5) = \frac{1}{2} \left[ 1 + \text{erf} \left( \frac{5 - \mathcal{M}_{\bullet}}{\delta\mathcal{M}_{\bullet}\sqrt{2}} \right) \right] \quad (7)$$

(Weisstein, 2002). Doing so for the mass estimate from equation (6), we find  $P(\mathcal{M}_{\bullet} \leq 5) = 65\%$ . We have additionally checked the pitch angle in alternative imaging that also traces star formation in spiral arms, by using the Galaxy Evolution Explorer (GALEX) far-ultraviolet (FUV) passband (1350–1750 Å). We found that the pitch angle from GALEX FUV imaging,  $27.5 \pm 3.9$ , is highly consistent with that from 8.0- $\mu\text{m}$  imaging.

## 2.2 The $M_{\bullet}$ - $M_{\text{gal},\star}$ relation

For our second estimate, we used the total stellar mass of NGC 3319 as a predictor of the black hole mass at its centre. We began by obtaining *Spitzer* images and masks for NGC 3319 from the S<sup>4</sup>G catalogue (Sheth et al., 2010).<sup>7</sup> We elected to use the 3.6  $\mu\text{m}, \star$  stellar image

<sup>7</sup><https://irsa.ipac.caltech.edu/data/SPITZER/S4G/index.html>

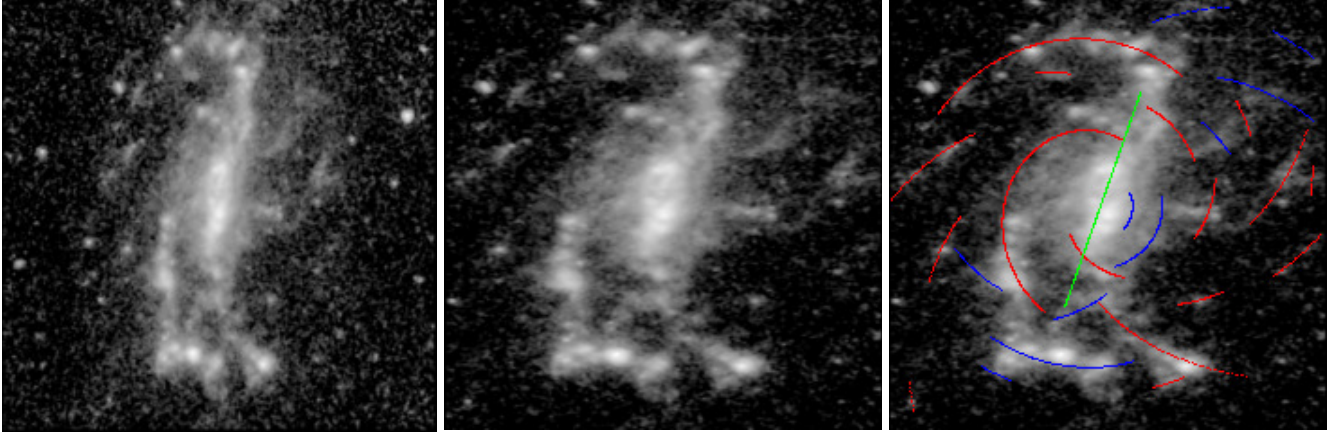


**Figure 2.** **Left (Original)** – *Spitzer* 8.0  $\mu\text{m}$  image of NGC 3319. Here, the image has been aligned, pointing the top of the image in the direction of the galaxy’s position angle ( $43^\circ 0$  east of north), and the image has been cropped into a square that is  $5' \times 5'$  ( $20.7 \text{ kpc} \times 20.7 \text{ kpc}$ ). **Middle (Deprojected)** – here, the original image has been deprojected to an artificial *face-on* orientation, achieved by stretching the X-axis by a factor of  $a/b \equiv (1 - \epsilon_{\text{outer}})^{-1} = 1.77$ , where  $a$  is the semi-major axis length, and  $b$  is the semi-minor axis length of the outer isophotes (Salo et al., 2015). **Right (Spiral Arcs)** – the spiral arcs measured by SPARCFIRE (Davis & Hayes, 2014) are overlaid upon the deprojected image. Fitted lines depict: (used) Z-wise spiral arcs (—), (ignored) S-wise spiral arcs (—), and the galactic bar (—). The reported pitch angle,  $31^\circ 7 \pm 4^\circ 5$ , is the weighted-mean pitch angle of the dominant-chirality red spiral arcs (see Section 2.1.1).

from Querejeta et al. (2015). The  $3.6 \mu\text{m}, \star$  image has been created after determining the amount of glowing dust present (by analysing the empirical  $3.6 \mu\text{m}$  and  $4.5 \mu\text{m}$  images) and subsequently subtracting the dust light from the  $3.6 \mu\text{m}$  image. Thus, the  $3.6 \mu\text{m}, \star$  image shows only the light emitted from the stellar population, and its luminosity can be directly converted into a stellar mass. We adopted a  $3.6 \mu\text{m}$  stellar mass-to-light ratio,  $\Upsilon_{3.6 \mu\text{m}, \star} = 0.60 \pm 0.09$  from Meidt et al. (2014),<sup>8</sup> along with a solar absolute magnitude,  $\mathfrak{M}_{3.6 \mu\text{m}, \odot} = 6.02 \text{ mag}$  (AB), at  $3.6 \mu\text{m}$  (Oh et al., 2008).

To model the light from NGC 3319, we utilised the isophotal fitting and modelling software routines ISOFIT and CMODEL (Ciambur, 2015), respectively. After masking extraneous light sources, we ran ISOFIT on the  $3.6 \mu\text{m}, \star$  image (Fig. 3, left panel) and used CMODEL to extract, and create a representation of, the galaxy (Fig. 3, second panel). The quality of the extraction can be seen in the residual images presented in the right two panels of Fig. 3.

The extracted galaxy was then analysed by the surface brightness profile fitting software PROFILER (Ciambur, 2016). This works by convolving the galaxy model with the *Spitzer* (IRAC channel 1) point spread function (PSF) with a full width at half maximum (FWHM) of  $1''.66$  for the cryogenic mission<sup>9</sup> until an optimal match

<sup>8</sup>The  $3.6 \mu\text{m}$  bandpass has a low uncertainty for the stellar mass-to-light ratio, with  $\Upsilon_{\star}$  from 0.40 to 0.55 (Schombert et al., 2019). This is consistent with the observed (i.e. with dust glow)  $\Upsilon_{3.6 \mu\text{m}, \star, \text{obs}} = 0.453 \pm 0.072$  value derived by Davis et al. (2019a, section 2.8), which is equivalent to the dust-corrected  $\Upsilon_{3.6 \mu\text{m}, \star} = 0.60 \pm 0.09$  from Meidt et al. (2014).

<sup>9</sup><https://irsa.ipac.caltech.edu/data/SPITZER/docs/irac/iracinstrumenthandbook/5/>

is achieved.<sup>10</sup> We present the resulting galaxy surface brightness profiles and multi-component fits for both the major axis (Fig. 4, left two panels) and the geometric mean axis, equivalent to a circularised representation of the galaxy (Fig. 4, right two panels).

We confirm that NGC 3319 is a bulgeless galaxy and does not require a traditional Sérsic bulge component (Sérsic, 1963; Ciotti, 1991; Graham & Driver, 2005). Instead, we generate a convincing fit that adequately captures all of the light of the galaxy (with a total rms scatter,  $\Delta_{rms} < 0.11 \text{ mag}$ ) using five components: a Ferrers bar (Ferrers, 1877); an exponential disk; two Gaussian components to capture spiral arm crossings of the major axis; and a point source at the centre. We calculate a total integrated  $3.6 \mu\text{m}, \star$  apparent magnitude of  $12.42 \pm 0.11 \text{ mag}$  (AB). Additional component magnitudes are tabulated in Table 1. Based on its distance ( $14.3 \pm 1.1 \text{ Mpc}$ ), we determine an absolute magnitude of  $-18.37 \pm 0.20 \text{ mag}$  for the galaxy at  $3.6 \mu\text{m}, \star$ . Applying  $\Upsilon_{3.6 \mu\text{m}, \star} = 0.60 \pm 0.09$  (Meidt et al., 2014) and  $\mathfrak{M}_{3.6 \mu\text{m}, \odot} = 6.02 \text{ mag}$  (AB) yields a total logarithmic

<sup>10</sup>PROFILER uses an unweighted least-squares Levenberg-Marquardt (Marquardt, 1963) algorithm (via PYTHON package LMFIT; Newville et al., 2016) to minimise the total rms scatter,

$$\Delta_{rms} = \sqrt{(n - f + 1)^{-1} \sum_{i=R_{\min}}^{R_{\max}} (\mu_{\text{data}, i} - \mu_{\text{model}, i})^2},$$

with surface brightnesses of the data (obtained from ISOFIT) and model, each at radial bin,  $i$ , where  $n$  is the number of radial bins (inclusive) between the minimum ( $R_{\min}$ ) and maximum ( $R_{\max}$ ) user-selected radii, and  $f$  is the number of free parameters (i.e. the number of user-selected components); PROFILER adjusts the model (summation of user-selected components) until a global minimum is reached. Additionally, a residual profile,  $\Delta\mu(R) = \mu_{\text{data}}(R) - \mu_{\text{model}}(R)$ , is provided in the output plots of PROFILER to demonstrate the quality of the fit as a function of galactocentric radius ( $R$ ).

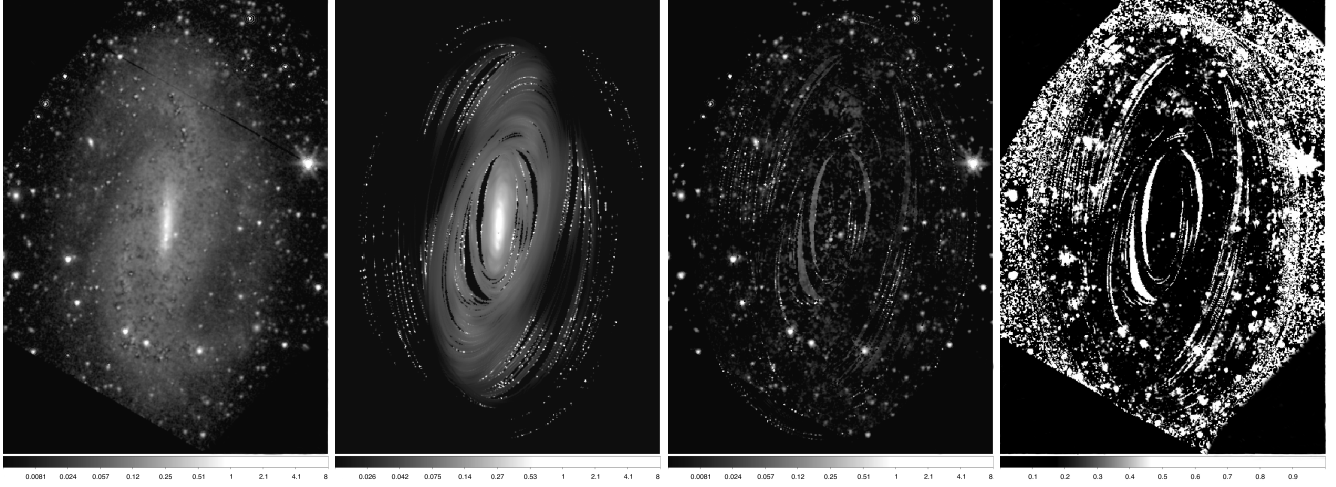


**Figure 3.** **Left (Original)** – *Spitzer*  $3.6\ \mu\text{m}, \star$  image of NGC 3319. Here, the image has been aligned so that the top of the image is pointing in the direction of the galaxy’s position angle ( $43^\circ 0$  east of north), and the image has been cropped, so it is  $5' \times 7'$  ( $20.7\ \text{kpc} \times 28.98\ \text{kpc}$ ). The black pixels indicate no intensity, and white pixels (pixel intensity of  $8.2\ \text{MJy sr}^{-1}$ ) indicate  $\mu_{3.6\ \mu\text{m}, \star} \leq 18.188\ \text{mag arcsec}^{-2}$ . **Second from Left (Model)** – model produced by ISOFIT and CMODEL (Ciambur, 2015), which includes a sky background of  $0.0180\ \text{MJy sr}^{-1}$  (Salo et al., 2015). **Second from Right (Residual)** – residual image, such that  $\text{Residual} \equiv \text{Original} - \text{Model}$ . **Right (Division)** – division image, such that  $\text{Division} \equiv \text{Residual} \div \text{Original}$ . The division image depicts the relative difference between the original and the residual image. Pixel values are between zero (black) and one (white), representing maximal and minimal change, respectively.

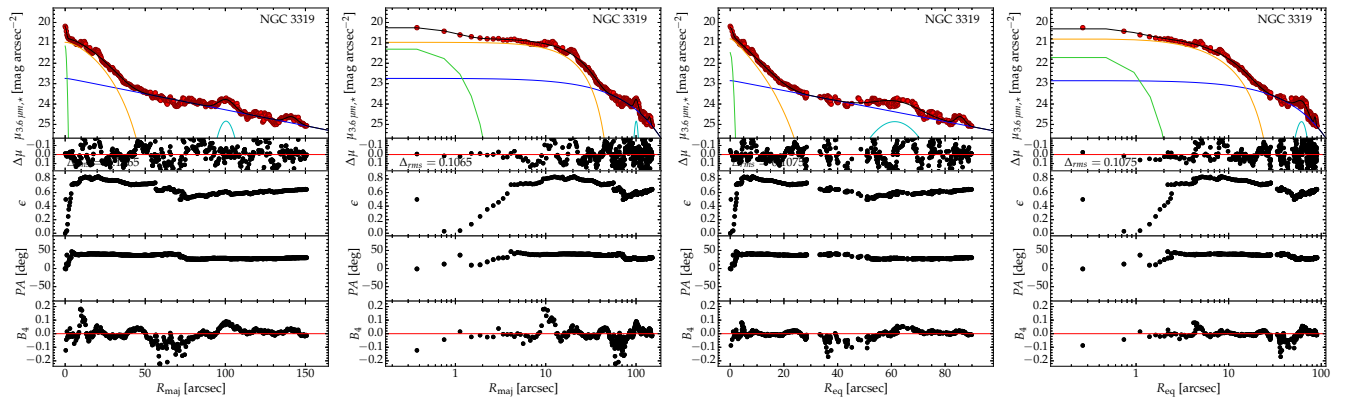


**Figure 4.** Surface brightness profile decompositions produced by PROFILER (Ciambur, 2016). **Panels (from left to right):** linear major-axis, log major-axis, linear equivalent-axis, and log equivalent-axis profiles;  $R_{\text{eq}} = \sqrt{ab} = R_{\text{maj}}\sqrt{1 - \epsilon}$  and  $R_{\text{maj}} \equiv a$ . **Subplots (from top to bottom):** surface brightness profile ( $\bullet$ ) and model ( $\text{—}$ ) built from the summation of the following components: PSF ( $\text{—}$ ), bar ( $\text{—}$ ), disk ( $\text{—}$ ), and spiral arms ( $\text{—}$ ), the faint outer spiral arm (at  $R_{\text{maj}} \approx 140'' \equiv R_{\text{eq}} \approx 85''$ ) lies below the plotted region; residual profile with total rms scatter ( $\Delta_{\text{rms}}$ ); ellipticity profile; position angle profile; and fourth-order cosine *Fourier* harmonic coefficient,  $B_4$  ( $B_2, B_3, B_6, B_8,$  and  $B_{10}$  harmonics are also fit and contribute to the model).

stellar mass of  $\mathcal{M}_{\text{gal},\star} = 9.53 \pm 0.10$  (cf. Georgiev et al., 2016,  $\mathcal{M}_{\text{gal},\star} = 9.53 \pm 0.16$ ) for NGC 3319.

Savorgnan et al. (2016) discovered a distinct red and blue sequence for early- and late-type galaxies in the  $M_{\bullet}-M_{\text{gal},\star}$  diagram, forming a revision to the core-Sérsic (giant early-type galaxies) and Sérsic (spiral and low-mass early-type galaxy) sequence from Graham (2012), Graham & Scott (2013), and Scott et al. (2013). van den Bosch (2016) subsequently showed this separation including additional galaxies, albeit with less reliable black hole masses, while Terrazas et al. (2016) captured it in terms of star formation rate. Here, we apply the latest relation established for spiral galaxies with directly-measured black hole masses. Applying equation 3 (with  $v \equiv 1$ ) from Davis et al. (2018), this total galaxy stellar mass predicts a central black hole mass as follows,

$$\mathcal{M}_{\text{gal},\star} = 9.53 \pm 0.10 \rightarrow \mathcal{M}_{\bullet}(M_{\text{gal},\star}) = 3.38 \pm 1.02, \quad (8)$$

with  $P(\mathcal{M}_{\bullet} \leq 5) = 94\%$ .

As can be seen in the images and from the ellipticity profile, there is no mistaking that NGC 3319 possesses a strong bar that accounts for most of the light from the inner  $R_{\text{maj}} \lesssim 30''$  ( $\lesssim 2.1$  kpc) region of the galaxy. There is no obvious evidence of a bulge (spheroid) component; thus, NGC 3319 is considered to be a bulgeless galaxy. Even if one were to describe the bar as a pseudobulge mistakenly, its logarithmic ‘bulge’ mass would only be  $\mathcal{M}_{\text{bulge},\star} = 8.62 \pm 0.23$  (see Table 1). If applied to the  $M_{\bullet}-M_{\text{bulge},\star}$  relation from Davis et al. (2019a, their equation 11), this would still comfortably predict an IMBH of  $\mathcal{M}_{\bullet} = 3.73 \pm 0.91$ , with  $P(\mathcal{M}_{\bullet} \leq 5) = 92\%$ .

### 2.3 The $M_{\bullet}-M_{\text{NC},\star}$ relation

From our surface brightness profile decomposition of NGC 3319, we extracted a central point source apparent magnitude of  $m_{3.6\mu\text{m},\star} = 20.22 \pm 0.32$ , yielding an absolute magnitude of  $\mathfrak{M}_{3.6\mu\text{m},\star} = -10.57 \pm 0.36$ . We will assume that this luminosity is due to the nuclear cluster (NC) of stars. Of course, some contribution of flux will come from the AGN. Therefore, we estimate an upper limit to the nuclear star cluster mass using  $\Upsilon_{3.6\mu\text{m},\star} = 0.60 \pm 0.09$  and  $\mathfrak{M}_{3.6\mu\text{m},\odot} = 6.02$  mag (AB), to give  $\mathcal{M}_{\text{NC},\star} \leq 6.41 \pm 0.16$ . We deem this to be a reasonable estimate since it lies between the recent estimates of  $\mathcal{M}_{\text{NC},\star} = 6.24 \pm 0.07$  (Georgiev & Böker, 2014; Georgiev et al., 2016) and  $\mathcal{M}_{\text{NC},\star} = 6.76 \pm 0.07$  (Jiang et al., 2018), both from *Hubble Space Telescope* imaging of NGC 3319.

Using the new  $M_{\bullet}-M_{\text{NC},\star}$  relation of Graham

(2020),<sup>11</sup> given by

$$\mathcal{M}_{\bullet}(M_{\text{NC},\star}) = (2.62 \pm 0.42) \log \left( \frac{M_{\text{NC},\star}}{10^{7.83} M_{\odot}} \right) + (8.22 \pm 0.20), \quad (9)$$

and with an intrinsic scatter of 1.31 dex. However, due to AGN contamination, we treat this as an upper-limit black hole mass estimate. Therefore, we predict the following black hole mass,

$$\mathcal{M}_{\text{NC},\star} \leq 6.41 \pm 0.16 \rightarrow \mathcal{M}_{\bullet}(M_{\text{NC},\star}) \leq 4.51 \pm 1.51, \quad (10)$$

with  $P(\mathcal{M}_{\bullet} \leq 5) \geq 63\%$ .

### 2.4 The $M_{\bullet}-v_{\text{rot}}$ relation

From HyperLeda<sup>12</sup> (Paturel et al., 2003), we adopted their apparent maximum rotation velocity of the gas,  $v_{\text{max,g}} = 84.33 \pm 1.80$  km s<sup>-1</sup> (homogenised value derived from 24 independent measurements), which is the observed maximum rotation velocity uncorrected for inclination effect. We then converted this to a maximum physical velocity rotation corrected for inclination ( $v_{\text{rot}}$ ) via

$$v_{\text{rot}} \equiv \frac{v_{\text{max,g}}}{\sin i_{\text{disk}}} = 102.21 \pm 2.20 \text{ km s}^{-1}. \quad (11)$$

Application of equation 10 from Davis et al. (2019b) gives

$$v_{\text{rot}} = 102.21 \pm 2.20 \text{ km s}^{-1} \rightarrow \mathcal{M}_{\bullet}(v_{\text{rot}}) = 3.90 \pm 0.59, \quad (12)$$

with  $P(\mathcal{M}_{\bullet} \leq 5) = 97\%$ .

### 2.5 The $M_{\bullet}-\sigma_0$ relation

We obtained the central stellar velocity dispersion from Ho et al. (2009) and utilised equation 2 from Sahu et al. (2019b) to predict a black hole mass as follows,

$$\sigma_0 = 87.4 \pm 9.2 \text{ km s}^{-1} \rightarrow \mathcal{M}_{\bullet}(\sigma_0) = 6.08 \pm 0.67, \quad (13)$$

with  $P(\mathcal{M}_{\bullet} \leq 5) = 5\%$ . This black hole mass estimate is the highest of all our estimates; it is our only discrete mass estimate of NGC 3319\* with  $\mathcal{M}_{\bullet} > 5.2$ .

Ho et al. (2009) presented a catalogue of pre-existing velocity dispersions, observed sometime between 1982 and 1990 (Ho et al., 1995). The measurements were weighted-mean dispersions from the blue- and red-side of the Double Spectrograph (Oke & Gunn, 1982) mounted at the Cassegrain focus of the Hale 5.08 m telescope at Palomar Observatory. However, Ho et al. (2009) found that the blue-side spectral resolution is insufficient to

<sup>11</sup>See also Graham (2016a) and equation 12 from Graham et al. (2019).

<sup>12</sup><http://leda.univ-lyon1.fr/>



**Table 1** NGC 3319 component magnitudes and masses. **Columns:** (1) Surface brightness profile component. (2)  $3.6\ \mu\text{m}, \star$  apparent magnitude (AB). (3)  $3.6\ \mu\text{m}, \star$  absolute magnitude (AB). (4) Logarithmic (solar) mass.

Component	$m_{3.6\ \mu\text{m}, \star}$ (mag)	$M_{3.6\ \mu\text{m}, \star}$ (mag)	$M_{\star}$ (dex)
(1)	(2)	(3)	(4)
PSF (NC)	$20.22 \pm 0.32$	$-10.57 \pm 0.36$	$6.41 \pm 0.16$
Bar	$14.70 \pm 0.53$	$-16.09 \pm 0.56$	$8.62 \pm 0.23$
Disk	$12.67 \pm 0.10$	$-18.12 \pm 0.20$	$9.43 \pm 0.10$
Inner Spiral	$15.20 \pm 0.10$	$-15.59 \pm 0.20$	$8.42 \pm 0.10$
Outer Spiral	$17.63 \pm 0.29$	$-13.16 \pm 0.34$	$7.45 \pm 0.05$
<b>Total</b>	<b><math>12.42 \pm 0.11</math></b>	<b><math>-18.37 \pm 0.20</math></b>	<b><math>9.53 \pm 0.10</math></b>

reliably measure dispersions for most of the later-type galaxies in their sample, as was the case for NGC 3319. Ho et al. (2009) only presented a red-side velocity dispersion for NGC 3319. Moreover, Ho et al. (1995) noted that for their observations of NGC 3319 ‘the continuum shape of its spectrum may be uncertain because of imperfect correction for spatial focus variations’.

Although Jiang et al. (2018) do present a spectrum of NGC 3319 (see their figure 5) from the *Sloan Digital Sky Survey* (*SDSS*), they do not report on the velocity dispersion. The *SDSS* Data Release 12 (Alam et al., 2015) states<sup>13</sup> that ‘best-fit velocity-dispersion values  $\lesssim 100\ \text{km s}^{-1}$  are below the resolution limit of the *SDSS* spectrograph and are to be regarded with caution’. Nonetheless, we have attempted to measure the velocity dispersion from the *SDSS* spectrum (Fig. 5) and found  $\sigma_0 = 99 \pm 9\ \text{km s}^{-1}$  (given the aforementioned resolution limit, this is likely an upper limit), albeit with a discrepant estimate of its recessional velocity. We found  $cz = 860 \pm 6\ \text{km s}^{-1}$ , which is markedly different from the *SDSS* value ( $cz = 713 \pm 5\ \text{km s}^{-1}$ ), or even the mean heliocentric radial velocity from HyperLeda ( $cz = 738 \pm 7\ \text{km s}^{-1}$ ). Although  $\sigma_0 \lesssim 100\ \text{km s}^{-1}$ , and is thusly suspicious, our measurement of  $\sigma_0 = 99 \pm 9\ \text{km s}^{-1}$  is consistent with the value from (Ho et al., 1995). Better spectral resolution should provide greater clarity as to the velocity dispersion of this galaxy, which might also be influenced by the nuclear star cluster.

## 2.6 The $M_{\bullet}$ – $L_{2-10\ \text{keV}}$ relation

Mayers et al. (2018) studied a sample of 30 AGN ( $z \leq 0.23$ ,  $L_{2-10\ \text{keV}} \geq 10^{40.8}\ \text{erg s}^{-1}$ , and  $M_{\bullet} \geq 5.45$ ), with black hole masses estimated via Bentz & Katz (2015) and reported a trend between black hole mass and X-ray luminosity. From 2–10 keV *CXO* observations of the nuclear point source in NGC 3319, Jiang et al. (2018) calculated a luminosity of  $L_{2-10\ \text{keV}} = 10^{39.0 \pm 0.1}\ \text{erg s}^{-1}$ . We applied the  $M_{\bullet}$ – $L_{2-10\ \text{keV}}$  relation of Mayers et al.

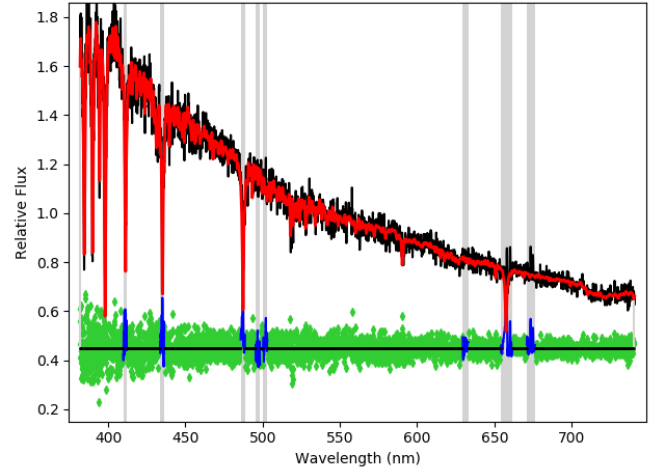


**Figure 5.** Fit to the *SDSS* spectrum of NGC 3319 by PXP (Cappellari, 2017). The relative flux of the observed spectrum (—) is over-plotted by the PXP fit (—) to the spectrum. The residuals to the fit (◆) are at the bottom (normalised about the arbitrary horizontal black line) along with residuals from the masked emission features (—), while grey vertical bands delineate the masked regions not included in the  $\chi^2$  minimisation of the fit. The fit is consistent with  $\sigma_0 = 99 \pm 9\ \text{km s}^{-1}$  and  $cz = 860 \pm 6\ \text{km s}^{-1}$ .

<sup>13</sup><https://www.sdss.org/dr12/algorithms/redshifts/>

(2018, extracted from their figure 11),

$$\mathcal{M}_\bullet(L_{2-10\text{keV}}) = (0.58 \pm 0.05) \log \left( \frac{L_{2-10\text{keV}}}{2 \times 10^{43} \text{ erg s}^{-1}} \right) + (7.46 \pm 0.34), \quad (14)$$

with a scatter of 0.89 dex, such that

$$L_{2-10\text{keV}} = 10^{39.0 \pm 0.1} \text{ erg s}^{-1} \rightarrow \mathcal{M}_\bullet(L_{2-10\text{keV}}) = 4.97 \pm 0.98, \quad (15)$$

with  $P(\mathcal{M}_\bullet \leq 5) = 51\%$ . However, given that the Eddington ratio will vary over time, as the AGN duty cycle turns the AGN on and off, this is unlikely to be a stable mass estimate.<sup>14</sup> The fundamental plane of black hole activity (Section 2.9) can offer additional insight, with its counterbalance from the waxing/waning radio emission.<sup>15</sup>

In what follows (Sections 2.7–2.9) are three black hole mass estimates from Jiang et al. (2018), which are explicitly described here.

## 2.7 The $M_\bullet$ – $\sigma_{\text{NXS}}^2$ relation

From the light curves obtained by the *CXO* observations, Jiang et al. (2018) estimated the X-ray variability, represented as the (10 ks) normalised excess variance ( $\sigma_{\text{NXS}}^2$ ). They found  $\sigma_{\text{NXS}}^2 = 0.093 \pm 0.088$ . By applying the  $M_\bullet$ – $\sigma_{\text{NXS}}^2$  relation from Pan et al. (2015, figure 4), Jiang et al. (2018) obtained

$$\sigma_{\text{NXS}}^2 = 0.093 \pm 0.088 \rightarrow \mathcal{M}_\bullet(\sigma_{\text{NXS}}^2) = 5.18 \pm 1.92, \quad (16)$$

with  $P(\mathcal{M}_\bullet \leq 5) = 46\%$ . Clearly, with an upper  $1\sigma$  estimate for the black hole mass of  $\sim 10^7 M_\odot$ , on its own this is not evidence for an IMBH.

## 2.8 Eddington ratio

Based upon the median radio-quiet quasar spectral energy distribution (SED) of Elvis et al. (1994), Jiang et al. (2018) determined a bolometric luminosity of  $L_{\text{bol}} = (3.6 \pm 1.1) \times 10^{40} \text{ erg s}^{-1}$  for NGC 3319\*, by scaling the SED to the *CXO* luminosity ( $L_{2-10\text{keV}} = 10^{39.0 \pm 0.1} \text{ erg s}^{-1}$ ) and integrating the entire SED. Using *XMM-Newton* and *CXO* observations of NGC 3319\*, Jiang et al. (2018) also determined a hard X-ray photon index of  $\Gamma = 2.02 \pm 0.27$ . Following Jiang et al.

<sup>14</sup>Woo & Urry (2002) found that the Eddington ratio for a given black hole can vary, spanning a range of up to three orders of magnitude. In order to be a stable relation, the  $M_\bullet$ – $L_{2-10\text{keV}}$  relation would require the time-varying distribution of Eddington ratios for a given black hole to resemble a normal distribution; several studies have found supportive evidence for a peaked distribution (Kollmeier et al., 2006; Steinhardt & Elvis, 2010; Lusso et al., 2012).

<sup>15</sup>Although, unmatched (in the radio) X-ray variability (typically not more than a factor of  $\approx 3$ ; Timlin et al., 2020) can possibly contribute to the scatter in the relation.

(2018), we converted this into an Eddington ratio,  $\log(L_{\text{bol}}/L_{\text{Edd}}) = -0.56 \pm 0.99$ , with an Eddington luminosity,  $L_{\text{Edd}} \equiv 1.26 \times 10^{38} M_\bullet (M_\odot^{-1} \text{ erg s}^{-1})$ , via equation 2 from Shemmer et al. (2008). Therefore,  $L_{\text{Edd}} = 10^{41.12 \pm 1.00} \text{ erg s}^{-1}$ .

From this point in the calculation, Jiang et al. (2018) arbitrarily selected  $L_{\text{bol}}/L_{\text{Edd}} = 0.1_{-0.099}^{+0.9}$ , implying  $M_\bullet = 3_{-2.7}^{+297} \times 10^3 M_\odot$ . Thus, Jiang et al. (2018) broadened the mass estimate to a range from  $M_\bullet = 3 \times 10^2$  to  $3 \times 10^5 M_\odot$  for arbitrary Eddington ratios ranging from 1 to  $10^{-3}$ , a range of 3 dex. For our purposes, we will remain with the calculated  $\log(L_{\text{bol}}/L_{\text{Edd}}) = -0.56$  with  $L_{\text{Edd}} = 10^{41.12} \text{ erg s}^{-1}$ , but will follow Jiang et al. (2018)’s conservative 3 dex range of uncertainty by broadening our estimate to

$$L_{\text{Edd}} = 10^{41.12 \pm 1.50} \text{ erg s}^{-1} \rightarrow \mathcal{M}_\bullet(L_{\text{Edd}}) = 3.02 \pm 1.50, \quad (17)$$

with  $P(\mathcal{M}_\bullet \leq 5) = 91\%$ .

## 2.9 Fundamental plane of black hole activity

Baldi et al. (2018) obtained high-resolution ( $\leq 0''.2$ ) 1.5 GHz-radio images of the core in NGC 3319 but failed to detect a source; therefore, establishing an upper limit to the luminosity,  $L_{1.5\text{GHz}} \leq 10^{35.03} \text{ erg s}^{-1}$ .<sup>16</sup> This radio luminosity can be applied to the fundamental plane of black hole activity (Merloni et al., 2003; Falcke et al., 2004; Gültekin et al., 2009; Plotkin et al., 2012; Dong & Wu, 2015; Liu et al., 2016; Nisbet & Best, 2016), which demonstrates an empirical correlation between the continuum X-ray, radio emission, and mass of an accreting black hole. This fundamental plane applies to supermassive, as well as stellar-mass black holes; therefore, it should also be suitable for the intervening population of IMBHs (e.g. Gültekin et al., 2014). Using the fundamental plane of black hole activity, Jiang et al. (2018) reported a black hole mass estimate of  $\leq 10^5 M_\odot$ . However, it is typically the 5 GHz, not the 1.5 GHz luminosity as we have, that is employed in the fundamental plane relation. Therefore, we follow the radiative flux density,  $S_\nu \propto \nu^{\alpha_R}$ , conversion of Qian et al. (2018) by adopting  $\alpha_R = -0.5 \pm 0.1$  as the typical radio spectral index of bright (high Eddington ratio) AGN. Doing so, this predicts an associated 5 GHz luminosity of  $L_{5\text{GHz}} \leq 10^{34.77 \pm 0.05} \text{ erg s}^{-1}$ . Using this value along with  $L_{2-10\text{keV}} = 10^{39.0 \pm 0.1} \text{ erg s}^{-1}$  (Section 2.6), we applied the relation of Gültekin et al. (2019, equation 8) to predict the following upper limit to the black hole mass,

$$\begin{aligned} L_{\text{FP}} &\equiv (L_{2-10\text{keV}}, L_{5\text{GHz}}) \\ &= (10^{39.0 \pm 0.1}, \leq 10^{34.77 \pm 0.05}) \text{ erg s}^{-1} \rightarrow \\ \mathcal{M}_\bullet(L_{\text{FP}}) &\leq 5.62 \pm 1.05, \end{aligned} \quad (18)$$

<sup>16</sup>Baldi et al. (2018) presented  $L_{1.5\text{GHz}} \leq 10^{34.84} \text{ erg s}^{-1}$  for NGC 3319, based on their adopted distance of 11.5 Mpc.

with  $P(\mathcal{M}_\bullet \leq 5) \geq 28\%$ .<sup>17</sup>

However, two issues make this particular prediction problematic. The first is that the radio and X-ray data were not obtained simultaneously, and the timescale for variations in flux will be short for IMBHs given that it scales with the size of the ‘event horizon’ and thus with the black hole mass. The second issue is that the ‘fundamental plane of black hole activity’ is applicable to black holes with low accretion rates (Merloni et al., 2003, their final paragraph of section 6), and NGC 3319\* is considered to have a high accretion rate (Jiang et al., 2018, see their section 3.2). Therefore, we do not include this estimate in our derivation of the black hole mass.

## 2.10 The $M_\bullet$ – $\mathcal{C}_{\text{FUV,tot}}$ relation

Dullo et al. (2020) present a relationship between the black hole mass and its host galaxy’s UV–3.6  $\mu\text{m}$  colour<sup>18</sup> from their study of 67 galaxies with directly-measured black hole masses. From table D1 in Dullo et al. (2020), the predicted black hole mass for NGC 3319\* is  $\mathcal{M}_\bullet = 5.36 \pm 0.85$ , based on its FUV–3.6  $\mu\text{m}$  colour ( $\mathcal{C}_{\text{FUV,tot}}$ ).<sup>19</sup> However, we can further refine this prediction by accounting for the internal dust extinction in NGC 3319. Given that NGC 3319 is bulgeless, we treat it as being all disk. Using our adopted inclination,  $i_{\text{disk}} = 55^\circ 6 \pm 0^\circ 2$ , and applying equations 2 and 4 from Dullo et al. (2020, see also Driver et al. 2008), we find that these corrections make NGC 3319  $0.57 \pm 0.16$  mag brighter in the ultraviolet and  $0.05 \pm 0.02$  mag brighter at 3.6  $\mu\text{m}$ .<sup>20</sup> Thus, the change in colour will be  $0.52 \pm 0.14$  mag bluer, which updates the FUV–3.6  $\mu\text{m}$  colour from Bouquin et al. (2018) to an internal-dust-corrected  $\mathcal{C}_{\text{FUV,tot}} = 1.16 \pm 0.14$  mag. Using the BCES bisector (Akritas & Bershadsky, 1996)  $M_\bullet$ – $\mathcal{C}_{\text{FUV,tot}}$  relation for late-type galaxies with a slope of  $1.03 \pm 0.13$  from ta-

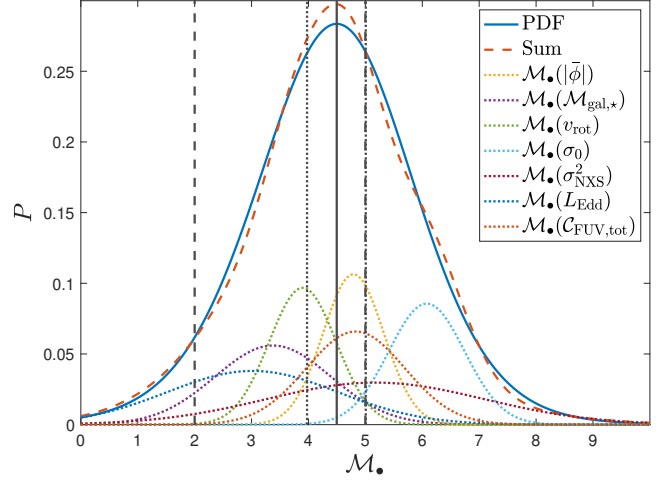


**Figure 6.** Determination of the PDF of the black hole mass estimates for NGC 3319\*. The PDF (—) is the best-fit skew-kurtotic-normal distribution to the Sum (---) of each of the seven selected black hole mass estimates’ normal distributions; --- = --- + --- + --- + --- + --- + --- + ---. The solid vertical line (—) indicates the position of  $\widehat{\mathcal{M}}_\bullet$ . The dotted vertical lines (.....) demarcate  $\widehat{\mathcal{M}}_\bullet - \delta^- \widehat{\mathcal{M}}_\bullet$  (left) and  $\widehat{\mathcal{M}}_\bullet + \delta^+ \widehat{\mathcal{M}}_\bullet$  (right, overlapping with the dashed line). The dashed vertical lines (---) demarcate the upper- and lower-bound mass definitions of an IMBH.

ble 2 in Dullo et al. (2020), we obtain a black hole mass which is  $1.03 \pm 0.13 \times 0.52 \pm 0.14 = 0.53 \pm 0.16$  dex smaller than reported in table D1. This revision reduces the tabulated estimate of  $\mathcal{M}_\bullet$  from  $5.36 \pm 0.85$  to  $4.83 \pm 0.87$ . Thus,

$$\begin{aligned} \mathcal{C}_{\text{FUV,tot}} &= 1.16 \pm 0.14 \text{ mag} \rightarrow \\ \mathcal{M}_\bullet(\mathcal{C}_{\text{FUV,tot}}) &= 4.83 \pm 0.87, \end{aligned} \quad (19)$$

with  $P(\mathcal{M}_\bullet \leq 5) = 58\%$ .

## 2.11 Probability density function

With such a multitude of mass estimates and a hesitancy to place confidence in one measurement alone, we combined the aforementioned mass estimates (except for that from equation 15) to yield a single black hole mass estimate for NGC 3319\*. We did so by analysing the probability density function (PDF) of the distribution of mass estimates (see Fig. 6). For our seven selected black hole mass estimates (equations 6, 8, 12, 13, 16, 17, and 19), we let a normal distribution represent each estimate with their respective means ( $\widehat{\mathcal{M}}_\bullet$ ) and standard deviations ( $\delta \widehat{\mathcal{M}}_\bullet$ ). We then added the seven Gaussians together to produce a combined summation. To ensure the area of the summation is equal to one, we divided each of the seven Gaussian addends by seven so that the area under each Gaussian equalled 1/7.

We fit a skew-kurtotic-normal distribution to the summation and measured the peak (mode) black hole mass

<sup>17</sup>Given the connection between the black hole mass estimates from the Eddington ratio (equation 17) and the fundamental plane (equation 18) we also check that the former ( $L_{2-10 \text{ keV}} = 10^{39.0 \pm 0.1} \text{ erg s}^{-1}$  and  $\mathcal{M}_\bullet(L_{\text{Edd}}) = 3.02 \pm 1.50$ ) is consistent with no radio detection ( $L_{5 \text{ GHz}} \leq 10^{34.77 \pm 0.05} \text{ erg s}^{-1}$ ). Using equation 19 from Gültekin et al. (2019), with the radio luminosity as the dependent variable in their regression, we find  $L_{5 \text{ GHz}} = 10^{33.76 \pm 1.41} \text{ erg s}^{-1}$ . Thus, the inverse prediction is consistent with no radio detection.

<sup>18</sup>See also the dependence of black hole mass on the colour of its host galaxy presented by Zasov & Cherepashchuk (2013).

<sup>19</sup>Dullo et al. (2020) also supply an  $M_\bullet$ – $\mathcal{C}_{\text{NUV,tot}}$  relation, but given the similarity with the  $M_\bullet$ – $\mathcal{C}_{\text{FUV,tot}}$  relation, we prefer to use the FUV relation due to its smaller uncertainty on the slope and intercept.

<sup>20</sup>We note the caveat that the relations of Dullo et al. (2020) are based on bulge plus disk magnitudes, not total galaxy magnitudes. In contrast, the colours from Bouquin et al. (2018), which were used to predict black hole masses in table D1 of Dullo et al. (2020), are derived from asymptotic magnitudes that may include additional fluxes from bars, rings, and nuclear components. For NGC 3319, we assume the bar and disk have the same colour and require the same dust correction because bars are just the inner parts of disks that have changed their orbits.

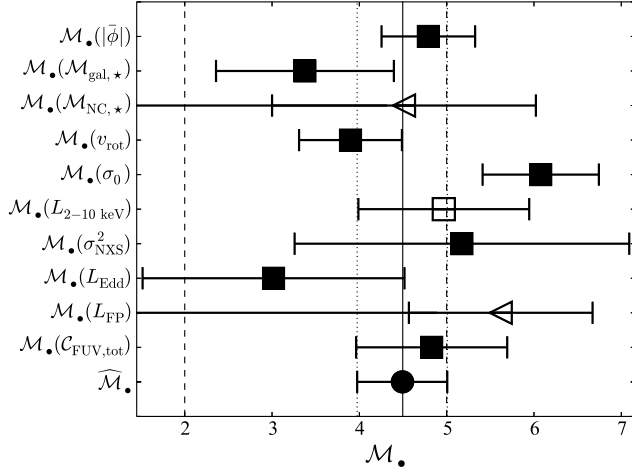


**Figure 7.** Forest plot of the ten different black hole mass estimates of NGC 3319\*. Seven discrete mass estimates (■) are used to generate the  $\widehat{M}_\bullet$  estimate (●) at the bottom of the figure. The black hole mass estimate from the X-ray luminosity,  $\mathcal{M}_\bullet(L_{2-10 \text{ keV}})$ , is plotted (□), but not included in the calculation of  $\widehat{M}_\bullet$ . Nor are the upper-limit black hole mass estimates included in the calculation of  $\widehat{M}_\bullet$ . The black hole mass estimates from the nuclear star cluster mass,  $\mathcal{M}_\bullet(\mathcal{M}_{\text{NC},*})$ , and the fundamental plane of black hole activity,  $\mathcal{M}_\bullet(L_{\text{FP}})$ , are upper-limit black hole mass estimates depicted by left-pointing open triangles (◁). The vertical lines are equivalent to those found in Fig. 6.

of the PDF as

$$\widehat{M}_\bullet \equiv \mathcal{M}_\bullet(\max P) = 4.50^{+0.51}_{-0.52}, \quad (20)$$

where  $\mathcal{M}_\bullet(\max P)$  is the black hole mass when the probability ( $P$ ) reaches its maximum ( $\max P = 0.272$ ). We quantify its standard error as

$$\begin{aligned} \delta^+ \widehat{M}_\bullet &\equiv \frac{\text{RWHM}}{\sqrt{2N \ln 2}} = 0.51 \quad \text{and} \\ \delta^- \widehat{M}_\bullet &\equiv \frac{\text{LWHM}}{\sqrt{2N \ln 2}} = 0.52, \end{aligned} \quad (21)$$

with right width at half max  $\text{RWHM} = 1.59 \text{ dex}$ , left width at half max  $\text{LWHM} = 1.63 \text{ dex}$ , the number of predictors  $N = 7$ , and  $P(\widehat{M}_\bullet \leq 5) = 84\%$ . For a complete comparison of all the mass estimates, see Table 2 and Fig. 7.

### 3 DISCUSSION

We have presented multiple mass estimates for NGC 3319\*, eight of which are discrete estimates, and two are upper limits (Sections 2.3 and 2.9). The non-detection of a nuclear source in the radio observations places an upper limit that is indeed higher than most of our other mass estimates. This missing radio detection begs for future deep, high spatial resolution radio (along with simultaneous X-ray) observations to provide an improved mass estimate for NGC 3319\* via the

fundamental plane of black hole activity. Nonetheless, the upper-limit mass estimate from the fundamental plane of black hole activity (equation 18) is in agreement with our other mass estimate derived from X-ray measurements (equation 15).

Amongst our numerous mass estimates, it is perhaps the most well-known black hole mass scaling relation ( $M_\bullet - \sigma_0$ ) that produces the highest mass estimate. Indeed, equation (13) provides the only mass estimate that is not consistent with  $M_\bullet \leq 5$ . It would be of interest to obtain a suitably high-spectral resolution measurement of  $\sigma_0$  for NGC 3319 to confirm or revise the solitary measurement that is (now) at least 31 years old. Although, it is not unprecedented to find a black hole that is anomalously under-massive with respect to the  $M_\bullet - \sigma_0$  relation (Zaw et al., 2020).

We have used the latest refinement of the  $M_\bullet - \sigma_0$  relation by Sahu et al. (2019b) to estimate the black hole mass. Building on Davis et al. (2017), Sahu et al. (2019b) have determined that  $M_\bullet \propto \sigma_0^{5.82 \pm 0.75}$  from an analysis of 46 spiral galaxies with central velocity dispersion measurements and directly-measured black hole masses. However, none of these galaxies have black hole masses below  $\sigma_0 \approx 100 \text{ km s}^{-1}$  ( $M_\bullet = 10^6 M_\odot$ ). Sahu et al. (2019b, their figure 2) have revealed a tendency for galaxies with central velocity dispersions less than  $\sim 100 \text{ km s}^{-1}$  to reside above the  $M_\bullet - \sigma_0$  relation defined by the galaxies with higher velocity dispersions and directly-measured black hole masses (i.e. spatially resolved kinematics, not reverberation mapping nor single-epoch spectra coupled with a constant virial  $f$ -factor). Therefore, should the velocity dispersion of NGC 3319 be lower than  $\sigma_0 \approx 100 \text{ km s}^{-1}$ , a shallower  $M_\bullet - \sigma_0$  relation than used here will be required.

Baldassare et al. (2020) demonstrated that extrapolations of the shallow  $M_\bullet - \sigma_0$  relation for ‘classical bulges’ from Kormendy & Ho (2013) appears (perhaps superficially) valid down to black hole masses of  $10^5 M_\odot$ , with black hole mass estimates derived from single-epoch spectroscopic (virial; with assumption of an  $f$ -factor to account for the unknown broadline region geometry) masses. If we exclude the  $M_\bullet - \sigma_0$  mass estimate altogether, our  $\widehat{M}_\bullet$  black hole mass estimate for NGC 3319\* (equation 20) becomes  $\widehat{M}_\bullet = 4.14^{+0.50}_{-0.49}$ , with  $P(\widehat{M}_\bullet \leq 5) = 96\%$ , based on the remaining six discrete measures used in Fig. 6. Additionally, if we treat the nuclear star cluster upper-limit mass estimate as a discrete estimate, we arrive at  $\widehat{M}_\bullet = 4.19^{+0.48}_{-0.47}$ , also with  $P(\widehat{M}_\bullet \leq 5) = 96\%$ . This is based again on seven measures, except now excluding the  $M_\bullet - \sigma_0$  and  $M_\bullet - L_X$  relation estimates, as well as the fundamental plane estimate.

**Table 2** NGC 3319\* mass predictions. **Columns:** (1) Black hole mass scaling relation predictor. (2) Logarithmic black hole (solar) mass. (3) Probability that NGC 3319\* is  $\leq 10^5 M_\odot$ , via equation (7).

Predictor	$\mathcal{M}_\bullet \pm \delta\mathcal{M}_\bullet$ (dex)	$P(\mathcal{M}_\bullet \leq 5)$ (%)
(1)	(2)	(3)
$ \phi  = 28^\circ 0 \pm 2^\circ 3$	$4.79 \pm 0.54$	65
$\mathcal{M}_{\text{gal},\star} = 9.53 \pm 0.10$	$3.38 \pm 1.02$	94
$\mathcal{M}_{\text{NC},\star} \leq 6.41 \pm 0.16$	$\leq 4.51 \pm 1.51^\dagger$	$\geq 63$
$v_{\text{rot}} = 102.21 \pm 2.20 \text{ km s}^{-1}$	$3.90 \pm 0.59$	97
$\sigma_0 = 87.4 \pm 9.2 \text{ km s}^{-1}$	$6.08 \pm 0.67$	5
$L_{2-10 \text{ keV}} = 10^{39.0 \pm 0.1} \text{ erg s}^{-1}$	$4.97 \pm 0.98^\dagger$	51
$\sigma_{\text{NXS}}^2 = 0.093 \pm 0.088$	$5.18 \pm 1.92$	46
$L_{\text{Edd}} = 10^{41.12 \pm 1.50} \text{ erg s}^{-1}$	$3.02 \pm 1.50$	91
$L_{\text{FP}} \equiv (L_{2-10 \text{ keV}}, L_{5 \text{ GHz}}) = (10^{39.0 \pm 0.1}, \leq 10^{34.77 \pm 0.05}) \text{ erg s}^{-1}$	$\leq 5.62 \pm 1.05^\dagger$	$\geq 28$
$\mathcal{C}_{\text{FUV,tot}} = 1.16 \pm 0.14 \text{ mag}$	$4.83 \pm 0.87$	58
<b>PDF</b>	<b><math>4.50^{+0.51}_{-0.52}</math></b>	<b>84</b>

<sup>†</sup> Excluded from the black hole mass PDF.

### 3.1 Similarity to the IMBH in LEDA 87300

The IMBH candidate in LEDA 87300 (RGG 118) has been proclaimed the ‘smallest’ reported in a galaxy nucleus<sup>21</sup> (Baldassare et al., 2015, 2017; Graham et al., 2016). We adopt the same redshift ( $z = 0.02647 \pm 0.00026$ ) as Graham et al. (2016), but instead invoke the latest cosmographic parameters ( $H_0 = 67.66 \pm 0.42 \text{ km s}^{-1} \text{ Mpc}^{-1}$ ,  $\Omega_\Lambda = 0.6889 \pm 0.0056$ , and  $\Omega_m = 0.3111 \pm 0.0056$ ) from Planck Collaboration et al. (2020, equation 28) to calculate a Hubble flow (comoving radial) distance of  $116.6 \pm 1.3 \text{ Mpc}$  (Wright, 2006). This adjustment yields a mass of  $\mathcal{M}_\bullet = 4.48^{+0.52}_{-0.69}$  for the IMBH (LEDA 87300\*) in LEDA 87300, as determined by Graham et al. (2016), with  $P(\mathcal{M}_\bullet \leq 5) = 84\%$ . This was based on a virial  $f$ -factor of 2.8 (Graham et al., 2011) and the assumption that the  $M_\bullet$ - $\sigma_0$  relation for AGN and quiescent galaxies can be extrapolated below  $10^6 M_\odot$ . Thus, the masses of NGC 3319\* and LEDA 87300\* are nearly identical,  $3.14^{+7.02}_{-2.20} \times 10^4 M_\odot$  and  $3.00^{+6.93}_{-2.38} \times 10^4 M_\odot$ , respectively. However, given the overlapping error bars associated with both black holes, the best we can conclude at this time is that their masses may be similar.

### 3.2 Environment and secular evolution

NGC 3319 is a relatively isolated galaxy in a group of four galaxies: NGC 3104, 3184, 3198, and 3319 (Tully, 1988). Its nearest neighbour at present is most likely NGC 3198. NGC 3198 is at a distance ( $d$ ) from us of  $14.5 \pm 1.3 \text{ Mpc}$  (Cepheid variable star distance from Kelson et al., 1999), J2000 right ascen-

sion ( $\alpha$ ) of  $10^{\text{h}}19^{\text{m}}55^{\text{s}}$ , and J2000 declination ( $\delta$ ) of  $+45^\circ 33' 09''$ , while NGC 3319 is at  $d = 14.3 \pm 1.1 \text{ Mpc}$ ,  $\alpha = 10^{\text{h}}39^{\text{m}}09^{\text{s}}.8$ , and  $\delta = +41^\circ 41' 15''.9$ . Based on the heliocentric spherical coordinates of each galaxy, the physical distance between galaxies is

$$\begin{aligned} \|\vec{d}_1 - \vec{d}_2\| \equiv & \sqrt{d_1^2 + d_2^2 - 2d_1d_2 \cos(\alpha_1 - \alpha_2)} \\ & - \sqrt{2d_1d_2 \sin \alpha_1 \sin \alpha_2 [\cos(\delta_1 - \delta_2) - 1]}. \end{aligned} \quad (22)$$

The physical separation between NGC 3198 and NGC 3319 is thus  $1.3 \pm 0.2 \text{ Mpc}$ .

With this level of isolation, NGC 3319 will likely experience many gigayears of relative tranquillity, without any significant galaxy mergers. If so, NGC 3319\* should continue to coevolve along with its host galaxy via secular accretion and feedback. There is no telling evidence that NGC 3319 has experienced a recent major merger. However, we do note that Moore & Gottesman (1998) detected a small system ( $4.2 \times 10^7 M_\odot$ ), just  $11'$  ( $46 \pm 4 \text{ kpc}$ ) south of NGC 3319. Moore & Gottesman (1998) postulate that tidal interactions between this object and NGC 3319 likely explain the distorted spiral structure, HI tail, and velocity perturbations in the southern half of the galaxy.

### 3.3 Direct measurements of NGC 3319\*

Stellar remnant black holes are thought to exist between the Tolman-Oppenheimer-Volkoff limit of  $\approx 2.17 M_\odot$  for cold, non-rotating neutron stars (Tolman, 1939; Oppenheimer & Volkoff, 1939; Margalit & Metzger, 2017; Shibata et al., 2017; Ruiz et al., 2018; Rezzolla et al., 2018) and  $\lesssim 60\text{--}80 M_\odot$  from the collapse of massive stars estimated from evolutionary models (Belczynski et al., 2010; Woosley, 2017; Spera & Mapelli, 2017). Recent observations have found the least massive known

<sup>21</sup>The first strong IMBH candidate is an off-centre ultra-luminous X-ray point source that is too bright to be an accreting stellar-mass black hole (Farrell et al., 2009).

black hole ( $\approx 3.3 M_{\odot}$ ; Thompson et al., 2019).<sup>22</sup> Over the past couple of years, black holes have been discovered that begin to surpass the low-mass definition of IMBHs:  $84.4_{-11.1}^{+15.8} M_{\odot}$  (Abbott et al., 2019a) and  $98_{-11}^{+17} M_{\odot}$  (Zackay et al., 2019). The gravitational-wave signal GW190521 (Abbott et al., 2020a) is consistent with the BH-collisional-creation of a  $142_{-16}^{+28} M_{\odot}$  IMBH. Its properties and astrophysical implications (Abbott et al., 2020b) are further remarkable given the high confidence that at least one of its progenitors lay in the mass gap predicted by pair-instability supernova theory (Woosley, 2017).<sup>23</sup>

The dwarf elliptical galaxy NGC 205 (M110), which is a satellite of the Andromeda Galaxy (M31), is presently the least massive nuclear black hole measured via direct methods. Nguyen et al. (2019) estimated a black hole mass of  $M_{\bullet} = 3.83_{-0.60}^{+0.43}$  via stellar dynamical modelling. Furthermore, this galaxy seemingly confirms the extrapolation of scaling relations into the IMBH regime. Explicitly, its black hole mass is consistent with the prediction,  $M_{\bullet}(\sigma_0) = 3.86 \pm 0.55$ , of the  $M_{\bullet}-\sigma_0$  relation (Sahu et al., 2019b, equation 1) with  $\sigma_0 = 33.1 \pm 4.8 \text{ km s}^{-1}$  from HyperLeda.

In order to dynamically estimate the mass of NGC 3319\*, it is necessary to resolve motions within its sphere of influence (SOI). According to Peebles (1972), the gravitational SOI of a black hole residing at the centre of a galaxy has a radius,

$$r_h \equiv \frac{GM_{\bullet}}{\sigma_0^2}. \quad (23)$$

Based on its (questionably high) velocity dispersion (equation 13), its  $\widehat{M}_{\bullet}$  black hole mass estimate (equation 20), and distance, we obtain  $r_h = 17.7_{-12.2}^{+40.8} \text{ mpc} = 255_{-176}^{+591} \mu\text{as}$  for NGC 3319\*.<sup>24</sup>

The Atacama Large Millimeter Array (ALMA) is useful for probing the gaseous cores of galaxies, including the rotating, torus-shaped, circumnuclear rings of molecular gas that enable measurements of the central black hole mass (e.g. García-Burillo et al., 2014; Yoon, 2017; Combes et al., 2019; Davis et al., 2020). ALMA currently has an impressive FWHM spatial resolution of 20 mas at 230 GHz. The East Asian VLBI Network (EAVN; see Wajima et al., 2016; Hada et al., 2017; An et al., 2018) has achieved a spatial resolution of 0.55 mas

<sup>22</sup>See also the recent  $3.04 \pm 0.06 M_{\odot}$  black hole candidate (Jayasinghe et al., 2021).

<sup>23</sup>Alternatively, Roupas & Kazanas (2019) propose that black holes between 50 and 135  $M_{\odot}$  can form via rapid gas accretion in primordial dense clusters.

<sup>24</sup>Because we question the discrepantly high  $\sigma_0$  value from equation 13, we alternatively can use the mass prediction of  $\widehat{M}_{\bullet} = 4.14_{-0.49}^{+0.50}$  (which does not consider equation 13) to predict  $\sigma_0$  from the  $M_{\bullet}-\sigma_0$  relation. Reversing the relation from Sahu et al. (2019b, equation 2), we find that  $\sigma_0 = 46.8 \pm 16.9 \text{ km s}^{-1}$ . Using this value now instead of the observed  $\sigma_0$ , equation 23 yields  $r_h = 27.4_{-16.5}^{+79.6} \text{ mpc} = 395_{-237}^{+1151} \mu\text{as}$  for NGC 3319\*.

(550  $\mu\text{as}$ ) at 22 GHz. Similar milliarcsecond-scale resolution can be expected from the Long Baseline Array (LBA; Edwards & Phillips, 2015) and the European VLBI Network (EVN; e.g. Radcliffe et al., 2018). The Very Long Baseline Array (VLBA) could likely resolve the SOI of NGC 3319\*, with its spatial resolution of 0.12 mas (120  $\mu\text{as}$ ) by utilising its longest baseline at 3 mm, currently between Mauna Kea, Hawaii and North Liberty, Iowa.<sup>25</sup> The Event Horizon Telescope (EHT) can also resolve the SOI of NGC 3319\*, with its PSF FWHM of 20  $\mu\text{as}$ . The EHT was able to resolve the emission ring, showing the event horizon, surrounding the SMBH M87\* with a diameter of  $42 \pm 3 \mu\text{as}$  (Event Horizon Telescope Collaboration et al., 2019).

Due to the difficulty of obtaining a direct measurement of the mass of NGC 3319\*, it would be prudent to first study the AGN in NGC 3319 via reverberation mapping (RM) methods. In this respect, the bulgeless spiral galaxy NGC 4395 is the prototype. NGC 4395 possesses one of the least massive nuclear black holes that has ever been measured via direct methods. den Brok et al. (2015) obtained a black hole mass estimate of  $4.0_{-1.0}^{+2.7} \times 10^5 M_{\odot}$  via gas dynamical modelling; Brum et al. (2019) similarly obtained  $2.5_{-0.8}^{+1.0} \times 10^5 M_{\odot}$  via gas kinematics. These direct measurements were preceded by informative RM black hole mass estimates of  $(3.6 \pm 1.1) \times 10^5 M_{\odot}$  (Peterson et al., 2005) and  $(4.9 \pm 2.6) \times 10^4 M_{\odot}$  (Edri et al., 2012, see also Cho et al. 2020 and Burke et al. 2020). Likewise, NGC 3319\* could greatly benefit from further study by RM campaigns, or at least single-epoch spectra mass estimates.

### 3.4 Implications

The abundance, or scarcity, of black holes in this new mass domain of IMBHs, has a broad array of implications. These include:

- Using low-mass AGN to extend the black hole scaling relations for predicting black hole masses in galaxies with quiescent low-mass black holes.
- IMBHs will enable further refinement of the  $M_{\bullet}-M_{\text{bulge},*}$  and  $M_{\bullet}-M_{\text{gal},*}$  diagrams (e.g. Davis et al., 2018, 2019a; Sahu et al., 2019a), further facilitating the advancement of BH/galaxy coevolution theories (e.g. Kauffmann & Haehnelt, 2000; Croton et al., 2006; Schaye et al., 2015).
- Establishing the black hole mass function from stellar to SMBHs, and then revising the black hole mass density of the Universe should IMBHs prove abundant (Aller & Richstone, 2002; Graham et al., 2007; Shankar et al., 2009; Davis et al., 2014; Mutlu-Pakdil et al., 2016).
- Increased understanding of the build-up of galaxies

<sup>25</sup><https://science.nrao.edu/facilities/vlba/docs/manuals/oss/ang-res>

in our hierarchical Universe via merger events, including IMBH mergers; searches for and constraints of merger rate densities for IMBH binaries (Abbott et al., 2019b; Jani et al., 2019).

- Connections with nuclear star clusters and ultra-compact dwarf galaxies (Graham & Spitler, 2009; Neumayer & Walcher, 2012; Georgiev et al., 2016; Nguyen et al., 2018; Graham, 2020; Neumayer et al., 2020) and predictions for space-based gravitational wave detections involving longer wavelength gravitational radiation than ground-based interferometers can detect (Portegies Zwart, 2007; Mapelli et al., 2012; Fragione & Silk, 2020). The much-anticipated Laser Interferometer Space Antenna (LISA; Amaro-Seoane et al., 2017) will have a designed observational requirement of detecting the coalescence of unequal mass black hole binaries of total intrinsic mass  $10^4$ – $10^6 M_{\odot}$  at  $z < 3$ . The merging of such black holes (similar to NGC 3319\*), each embedded in their nuclear star cluster, should coalesce within a Hubble time due to dynamical friction (Ogiya et al., 2020). LISA and the next generation of gravitational wave observatories should also be able to find IMBHs in Milky Way globular clusters and the Local Volume (Arca-Sedda et al., 2020).
- The violent tidal disruption of white dwarf stars by IMBHs can trigger calcium-rich supernovae, spurring the nucleosynthesis of iron-group elements, and are capable of generating observable electromagnetic and gravitational-wave energies (Rees, 1988; Haas et al., 2012; MacLeod et al., 2016; Andreoni et al., 2017, 2020; Kuns et al., 2020; Anninos et al., 2019; Malyali et al., 2019).

IMBHs represent the grail lemma, needed to fill the void in our demographic knowledge of black holes, and tie up our inadequate theoretical understanding of BH/galaxy coevolution, feedback, and the growth of the Universe’s most massive black holes. Increased future study of NGC 3319\* promises to yield direct confirmation of the existence of an IMBH in AGN mode and offer immediate and lasting scientific advancement.

## ACKNOWLEDGEMENTS

We are grateful to Jonah S. Gannon, who provided valuable expertise with the spectroscopic analysis. BLD thanks David Nelson for the use of his secluded office space during the COVID-19 pandemic. This research was supported by the Australian Research Council’s funding scheme DP17012923. Parts of this research were conducted by the Australian Research Council Centre of Excellence for Gravitational Wave Discovery (OzGrav), through project number CE170100004. This material is based upon work supported by Tamkeen under the NYU Abu Dhabi Research Institute

grant CAP<sup>3</sup>. This research has made use of NASA’s Astrophysics Data System, and the NASA/IPAC Extragalactic Database (NED) and Infrared Science Archive (IRSA). We acknowledge the use of the HyperLeda database (<http://leda.univ-lyon1.fr>). We made use of the DS9 visualization tool (Joye & Mandel, 2003), part of NASA’s High Energy Astrophysics Science Archive Research Center (HEASARC) software.

## REFERENCES

- Abbott B. P., et al., 2019a, *Phys. Rev. X*, 9, 031040  
 Abbott B. P., et al., 2019b, *Phys. Rev. D*, 100, 064064  
 Abbott R., et al., 2020a, *Phys. Rev. Lett.*, 125, 101102  
 Abbott R., et al., 2020b, *ApJ*, 900, L13  
 Abdeen S., Kennefick D., Kennefick J., Miller R., Shields D. W., Monson E. B., Davis B. L., 2020, *MNRAS*, 496, 1610  
 Abramowicz M. A., Calvani M., Nobili L., 1980, *ApJ*, 242, 772  
 Akritas M. G., Bershadsky M. A., 1996, *ApJ*, 470, 706  
 Alam S., et al., 2015, *ApJS*, 219, 12  
 Alexander T., Natarajan P., 2014, *Science*, 345, 1330  
 Alistair Seguel P. J., Schleicher D. R. G., Boekholt T. C. N., Fellhauer M., Klessen R. S., 2020, *MNRAS*, 493, 2352  
 Aller M. C., Richstone D., 2002, *AJ*, 124, 3035  
 Amaro-Seoane P., et al., 2017, arXiv e-prints, p. arXiv:1702.00786  
 An T., Sohn B. W., Imai H., 2018, *Nature Astronomy*, 2, 118  
 Andreoni I., Jacobs C., Hegarty S., Pritchard T., Cooke J., Ryder S., 2017, *PASA*, 34, e037  
 Andreoni I., et al., 2020, *MNRAS*, 491, 5852  
 Anninos P., Hoffman R. D., Grewal M., Lavell M. J., Fragile P. C., 2019, *ApJ*, 885, 136  
 Arca-Sedda M., Amaro-Seoane P., Chen X., 2020, arXiv e-prints, p. arXiv:2007.13746  
 Baldassare V. F., Reines A. E., Gallo E., Greene J. E., 2015, *ApJ*, 809, L14  
 Baldassare V. F., Reines A. E., Gallo E., Greene J. E., 2017, *ApJ*, 850, 196  
 Baldassare V. F., Dickey C., Geha M., Reines A. E., 2020, *ApJ*, 898, L3  
 Baldi R. D., et al., 2018, *MNRAS*, 476, 3478  
 Baldwin J. A., Phillips M. M., Terlevich R., 1981, *PASP*, 93, 5  
 Barrows R. S., Mezcua M., Comerford J. M., 2019, *ApJ*, 882, 181  
 Belczynski K., Bulik T., Fryer C. L., Ruiter A., Valsecchi F., Vink J. S., Hurley J. R., 2010, *ApJ*, 714, 1217  
 Bellovary J. M., et al., 2021, arXiv e-prints, p. arXiv:2102.09566  
 Bentz M. C., Katz S., 2015, *PASP*, 127, 67

- Berrier J. C., et al., 2013, *ApJ*, **769**, 132
- Bi S., Feng H., Ho L. C., 2020, *ApJ*, **900**, 124
- Bouquin A. Y. K., et al., 2018, *ApJS*, **234**, 18
- Bromm V., Loeb A., 2003, in Holt S. H., Reynolds C. S., eds, American Institute of Physics Conference Series Vol. 666, The Emergence of Cosmic Structure. pp 73–84 ([arXiv:astro-ph/0301406](https://arxiv.org/abs/astro-ph/0301406)), doi:10.1063/1.1581773
- Brum C., et al., 2019, *MNRAS*, **486**, 691
- Burke C. J., Shen Y., Chen Y.-C., Scaringi S., Faucher-Giguere C.-A., Liu X., Yang Q., 2020, *ApJ*, **899**, 136
- Cappellari M., 2017, *MNRAS*, **466**, 798
- Chilingarian I. V., Katkov I. Y., Zolotukhin I. Y., Grishin K. A., Beletsky Y., Boutsia K., Osip D. J., 2018, *ApJ*, **863**, 1
- Cho H., et al., 2020, *ApJ*, **892**, 93
- Ciambur B. C., 2015, *ApJ*, **810**, 120
- Ciambur B. C., 2016, *PASA*, **33**, e062
- Ciotti L., 1991, *A&A*, **249**, 99
- Combes F., et al., 2019, *A&A*, **623**, A79
- Croton D. J., et al., 2006, *MNRAS*, **365**, 11
- D’Onghia E., Vogelsberger M., Hernquist L., 2013, *ApJ*, **766**, 34
- Davies M. B., Miller M. C., Bellovary J. M., 2011, *ApJ*, **740**, L42
- Davis D. R., Hayes W. B., 2014, *ApJ*, **790**, 87
- Davis B. L., Berrier J. C., Shields D. W., Kenefick J., Kenefick D., Seigar M. S., Lacy C. H. S., Puerari I., 2012, *ApJS*, **199**, 33
- Davis B. L., et al., 2014, *ApJ*, **789**, 124
- Davis B. L., et al., 2015, *ApJ*, **802**, L13
- Davis B. L., Berrier J. C., Shields D. W., Kenefick J., Kenefick D., Seigar M. S., Lacy C. H. S., Puerari I., 2016, 2DFFT: Measuring Galactic Spiral Arm Pitch Angle (ascl:1608.015)
- Davis B. L., Graham A. W., Seigar M. S., 2017, *MNRAS*, **471**, 2187
- Davis B. L., Graham A. W., Cameron E., 2018, *ApJ*, **869**, 113
- Davis B. L., Graham A. W., Cameron E., 2019a, *ApJ*, **873**, 85
- Davis B. L., Graham A. W., Combes F., 2019b, *ApJ*, **877**, 64
- Davis T. A., et al., 2020, *MNRAS*, **496**, 4061
- Dong A.-J., Wu Q., 2015, *MNRAS*, **453**, 3447
- Driver S. P., Popescu C. C., Tuffs R. J., Graham A. W., Liske J., Baldry I., 2008, *ApJ*, **678**, L101
- Dullo B. T., Bouquin A. Y. K., Gil de Paz A., Knapen J. H., Gorgas J., 2020, *ApJ*, **898**, 83
- Eddington A. S., 1925, *MNRAS*, **85**, 408
- Edri H., Rafter S. E., Chelouche D., Kaspi S., Behar E., 2012, *ApJ*, **756**, 73
- Edwards P. G., Phillips C., 2015, Publication of Korean Astronomical Society, **30**, 659
- Elvis M., et al., 1994, *ApJS*, **95**, 1
- Event Horizon Telescope Collaboration et al., 2019, *ApJ*, **875**, L1
- Falcke H., Körding E., Markoff S., 2004, *A&A*, **414**, 895
- Farrell S. A., Webb N. A., Barret D., Godet O., Rodrigues J. M., 2009, *Nature*, **460**, 73
- Feng H., Soria R., 2011, *New Astron. Rev.*, **55**, 166
- Ferrers N., 1877, *QJ Pure Appl. Math*, **14**, 1
- Fragione G., Silk J., 2020, *MNRAS*, **498**, 4591
- García-Burillo S., et al., 2014, *A&A*, **567**, A125
- Georgiev I. Y., Böker T., 2014, *MNRAS*, **441**, 3570
- Georgiev I. Y., Böker T., Leigh N., Lützgendorf N., Neumayer N., 2016, *MNRAS*, **457**, 2122
- Graham A. W., 2012, *ApJ*, **746**, 113
- Graham A. W., 2016a, in Meiron Y., Li S., Liu F. K., Spurzem R., eds, IAU Symposium Vol. 312, Star Clusters and Black Holes in Galaxies across Cosmic Time. pp 269–273 ([arXiv:1412.5715](https://arxiv.org/abs/1412.5715)), doi:10.1017/S1743921315008017
- Graham A. W., 2016b, Galaxy Bulges and Their Massive Black Holes: A Review. Springer International Publishing Switzerland, p. 263, doi:10.1007/978-3-319-19378-6\_11
- Graham A. W., 2020, *MNRAS*, **492**, 3263
- Graham A. W., Driver S. P., 2005, *PASA*, **22**, 118
- Graham A. W., Scott N., 2013, *ApJ*, **764**, 151
- Graham A. W., Scott N., 2015, *ApJ*, **798**, 54
- Graham A. W., Soria R., 2019, *MNRAS*, **484**, 794
- Graham A. W., Spitler L. R., 2009, *MNRAS*, **397**, 2148
- Graham A. W., Driver S. P., Allen P. D., Liske J., 2007, *MNRAS*, **378**, 198
- Graham A. W., Onken C. A., Athanassoula E., Combes F., 2011, *MNRAS*, **412**, 2211
- Graham A. W., Ciambur B. C., Soria R., 2016, *ApJ*, **818**, 172
- Graham A. W., Soria R., Davis B. L., 2019, *MNRAS*, **484**, 814
- Griv E., Gedalin M., Shih I. C., Hou L.-G., Jiang I.-G., 2020, *MNRAS*, **493**, 2111
- Griv E., Gedalin M., Jiang I.-G., 2021, *MNRAS*, **503**, 354
- Grobov A. V., Rubin S. G., Samarchenko D. A., Zhizhin E. D., 2011, *Gravitation and Cosmology*, **17**, 181
- Gültekin K., Cackett E. M., Miller J. M., Di Matteo T., Markoff S., Richstone D. O., 2009, *ApJ*, **706**, 404
- Gültekin K., Cackett E. M., King A. L., Miller J. M., Pinkney J., 2014, *ApJ*, **788**, L22
- Gültekin K., King A. L., Cackett E. M., Nyland K., Miller J. M., Di Matteo T., Markoff S., Rupen M. P., 2019, *ApJ*, **871**, 80
- Haas R., Shcherbakov R. V., Bode T., Laguna P., 2012, *ApJ*, **749**, 117



- Hada K., et al., 2017, *PASJ*, **69**, 71
- Heckman T. M., 1980, *A&A*, **500**, 187
- Heckman T. M., Balick B., Crane P. C., 1980, *A&AS*, **40**, 295
- Ho L. C., Filippenko A. V., Sargent W. L., 1995, *ApJS*, **98**, 477
- Ho L. C., Filippenko A. V., Sargent W. L. W., 1997, *ApJS*, **112**, 315
- Ho L. C., Greene J. E., Filippenko A. V., Sargent W. L. W., 2009, *ApJS*, **183**, 1
- Inayoshi K., Haiman Z., Ostriker J. P., 2016, *MNRAS*, **459**, 3738
- Inayoshi K., Visbal E., Haiman Z., 2020, *ARA&A*, **58**, 27
- Jani K., Shoemaker D., Cutler C., 2019, *Nature Astronomy*, **4**, 260
- Jayasinghe T., et al., 2021, *MNRAS*, **504**, 2577
- Jiang Y.-F., Stone J. M., Davis S. W., 2014, *ApJ*, **796**, 106
- Jiang N., et al., 2018, *ApJ*, **869**, 49
- Joye W. A., Mandel E., 2003, in Payne H. E., Jędrzejewski R. I., Hook R. N., eds, *Astronomical Society of the Pacific Conference Series Vol. 295, Astronomical Data Analysis Software and Systems XII*. p. 489
- Kaaret P., Feng H., Roberts T. P., 2017, *ARA&A*, **55**, 303
- Kauffmann G., Haehnelt M., 2000, *MNRAS*, **311**, 576
- Kelson D. D., et al., 1999, *ApJ*, **514**, 614
- Kızıltan B., Baumgardt H., Loeb A., 2017, *Nature*, **542**, 203
- Koliopanos F., 2017, in *XII Multifrequency Behaviour of High Energy Cosmic Sources Workshop (MULTIF2017)*. p. 51 ([arXiv:1801.01095](https://arxiv.org/abs/1801.01095))
- Koliopanos F., et al., 2017, *A&A*, **601**, A20
- Kollmeier J. A., et al., 2006, *ApJ*, **648**, 128
- Kormendy J., Ho L. C., 2013, *ARA&A*, **51**, 511
- Kuns K. A., Yu H., Chen Y., Adhikari R. X., 2020, *Phys. Rev. D*, **102**, 043001
- Lin C. C., Shu F. H., 1964, *ApJ*, **140**, 646
- Lin C. C., Shu F. H., 1966, *Proceedings of the National Academy of Science*, **55**, 229
- Lin C. C., Yuan C., Shu F. H., 1969, *ApJ*, **155**, 721
- Lin D., et al., 2020, *ApJ*, **892**, L25
- Liu X., Han Z., Zhang Z., 2016, *Ap&SS*, **361**, 9
- Lupi A., Colpi M., Devecchi B., Galanti G., Volonteri M., 2014, *MNRAS*, **442**, 3616
- Lusso E., et al., 2012, *MNRAS*, **425**, 623
- MacLeod M., Guillochon J., Ramirez-Ruiz E., Kasen D., Rosswog S., 2016, *ApJ*, **819**, 3
- Madau P., Rees M. J., 2001, *ApJ*, **551**, L27
- Malyali A., Rau A., Nandra K., 2019, *MNRAS*, **489**, 5413
- Mapelli M., Ripamonti E., Vecchio A., Graham A. W., Gualandris A., 2012, *A&A*, **542**, A102
- Margalit B., Metzger B. D., 2017, *ApJ*, **850**, L19
- Marquardt D. W., 1963, *Journal of the Society for Industrial and Applied Mathematics*, **11**, 431
- Mayer L., Kazantzidis S., Escala A., Callegari S., 2010, *Nature*, **466**, 1082
- Mayers J. A., et al., 2018, *arXiv e-prints*, p. [arXiv:1803.06891](https://arxiv.org/abs/1803.06891)
- Meidt S. E., et al., 2014, *ApJ*, **788**, 144
- Merloni A., Heinz S., di Matteo T., 2003, *MNRAS*, **345**, 1057
- Mezcua M., 2017, *International Journal of Modern Physics D*, **26**, 1730021
- Mezcua M., Civano F., Marchesi S., Suh H., Fabbiano G., Volonteri M., 2018, *MNRAS*, **478**, 2576
- Mignoli M., et al., 2020, *A&A*, **642**, L1
- Miller M. C., Colbert E. J. M., 2004, *International Journal of Modern Physics D*, **13**, 1
- Miller R., Kennefick D., Kennefick J., Shameer Abdeen M., Monson E., Eufrazio R. T., Shields D. W., Davis B. L., 2019, *ApJ*, **874**, 177
- Moore E. M., Gottesman S. T., 1998, *MNRAS*, **294**, 353
- Mortlock D. J., et al., 2011, *Nature*, **474**, 616
- Mutlu-Pakdil B., Seigar M. S., Davis B. L., 2016, *ApJ*, **830**, 117
- Mutlu-Pakdil B., Seigar M. S., Hewitt I. B., Treuthardt P., Berrier J. C., Koval L. E., 2018, *MNRAS*, **474**, 2594
- Natarajan P., 2021, *MNRAS*, **501**, 1413
- Nayakshin S., Power C., King A. R., 2012, *ApJ*, **753**, 15
- Neumayer N., Walcher C. J., 2012, *Advances in Astronomy*, **2012**, 709038
- Neumayer N., Seth A., Böker T., 2020, *A&A Rev.*, **28**, 4
- Newville M., Stensitzki T., Allen D. B., Rawlik M., Ingarciola A., Nelson A., 2016, *Lmfit: Non-Linear Least-Square Minimization and Curve-Fitting for Python* ([ascl:1606.014](https://ascl.net/1606.014))
- Nguyen D. D., et al., 2017, *ApJ*, **836**, 237
- Nguyen D. D., et al., 2018, *ApJ*, **858**, 118
- Nguyen D. D., et al., 2019, *ApJ*, **872**, 104
- Nisbet D. M., Best P. N., 2016, *MNRAS*, **455**, 2551
- Ogiya G., Hahn O., Mingarelli C. M. F., Volonteri M., 2020, *MNRAS*, **493**, 3676
- Oh S.-H., de Blok W. J. G., Walter F., Brinks E., Kenicutt Robert C. J., 2008, *AJ*, **136**, 2761
- Oke J. B., 1974, *ApJS*, **27**, 21
- Oke J. B., Gunn J. E., 1982, *PASP*, **94**, 586
- Onken C. A., Ferrarese L., Merritt D., Peterson B. M., Pogge R. W., Vestergaard M., Wandel A., 2004, *ApJ*, **615**, 645
- Oppenheimer J. R., Volkoff G. M., 1939, *Physical Review*, **55**, 374
- Pan H.-W., Yuan W., Zhou X.-L., Dong X.-B., Liu B.,

- 2015, *ApJ*, **808**, 163
- Patuarel G., Theureau G., Bottinelli L., Gouguenheim L., Coudreau-Durand N., Hallet N., Petit C., 2003, *A&A*, **412**, 57
- Peebles P. J. E., 1972, *ApJ*, **178**, 371
- Peterken T. G., Merrifield M. R., Aragón-Salamanca A., Drory N., Krawczyk C. M., Masters K. L., Weijmans A.-M., Westfall K. B., 2019, *Nature Astronomy*, **3**, 178
- Peterson B. M., et al., 2005, *ApJ*, **632**, 799
- Pezzulli E., Valiante R., Schneider R., 2016, *MNRAS*, **458**, 3047
- Planck Collaboration et al., 2020, *A&A*, **641**, A6
- Plotkin R. M., Markoff S., Kelly B. C., K rding E., Anderson S. F., 2012, *MNRAS*, **419**, 267
- Pogge R. W., 1989, *ApJS*, **71**, 433
- Portegies Zwart S. F., 2007, *Advances in Space Research*, **39**, 275
- Portegies Zwart S. F., McMillan S. L. W., 2002, *ApJ*, **576**, 899
- Pour-Imani H., Kennefick D., Kennefick J., Davis B. L., Shields D. W., Shameer Abdeen M., 2016, *ApJ*, **827**, L2
- Qian L., Dong X.-B., Xie F.-G., Liu W., Li D., 2018, *ApJ*, **860**, 134
- Querejeta M., et al., 2015, *ApJS*, **219**, 5
- Radcliffe J. F., et al., 2018, *A&A*, **619**, A48
- Randriamampandry T. H., Combes F., Carignan C., Deg N., 2015, *MNRAS*, **454**, 3743
- Rees M. J., 1988, *Nature*, **333**, 523
- Rezzolla L., Most E. R., Weih L. R., 2018, *ApJ*, **852**, L25
- Roupas Z., Kazanas D., 2019, *A&A*, **632**, L8
- Ruiz M., Shapiro S. L., Tsokaros A., 2018, *Phys. Rev. D*, **97**, 021501
- Sahu N., Graham A. W., Davis B. L., 2019a, *ApJ*, **876**, 155
- Sahu N., Graham A. W., Davis B. L., 2019b, *ApJ*, **887**, 10
- Sakai S., et al., 1999, *ApJ*, **523**, 540
- Salo H., et al., 2015, *ApJS*, **219**, 4
- Savorgnan G. A. D., Graham A. W., Marconi A. r., Sani E., 2016, *ApJ*, **817**, 21
- Schaye J., et al., 2015, *MNRAS*, **446**, 521
- Schneider R., Ferrara A., Natarajan P., Omukai K., 2002, *ApJ*, **571**, 30
- Schombert J., McGaugh S., Lelli F., 2019, *MNRAS*, **483**, 1496
- Scott N., Graham A. W., Schombert J., 2013, *ApJ*, **768**, 76
- Secrest N. J., Satyapal S., Gliozzi M., Cheung C. C., Seth A. C., B ker T., 2012, *ApJ*, **753**, 38
- Seigar M. S., Bullock J. S., Barth A. J., Ho L. C., 2006, *ApJ*, **645**, 1012
- Seigar M. S., Kennefick D., Kennefick J., Lacy C. H. S., 2008, *ApJ*, **678**, L93
- Seigar M. S., Davis B. L., Berrier J., Kennefick D., 2014, *ApJ*, **795**, 90
- Seigar M. S., Mutlu-Pakdil B., Hewitt I. B., Treuhardt P., 2018, P2DFFT: Parallelized technique for measuring galactic spiral arm pitch angles (ascl:1806.011)
- S rsic J. L., 1963, Bolet n de la Asociaci n Argentina de Astronom a La Plata Argentina, **6**, 41
- Shankar F., Salucci P., Granato G. L., De Zotti G., Danese L., 2004, *MNRAS*, **354**, 1020
- Shankar F., Weinberg D. H., Miralda-Escud  J., 2009, *ApJ*, **690**, 20
- Shemmer O., Netzer H., Maiolino R., Oliva E., Croom S., Corbett E., di Fabrizio L., 2004, *ApJ*, **614**, 547
- Shemmer O., Brandt W. N., Netzer H., Maiolino R., Kaspi S., 2008, *ApJ*, **682**, 81
- Sheth K., et al., 2010, *PASP*, **122**, 1397
- Shibata M., Fujibayashi S., Hotokezaka K., Kiuchi K., Kyutoku K., Sekiguchi Y., Tanaka M., 2017, *Phys. Rev. D*, **96**, 123012
- Shields D. W., et al., 2015a, arXiv e-prints, p. arXiv:1511.06365
- Shields D. W., et al., 2015b, Spirality: Spiral arm pitch angle measurement (ascl:1512.015)
- Soltan A., 1982, *MNRAS*, **200**, 115
- Soria R., 2016, Spiral galaxies of the Virgo cluster, Chandra Proposal
- Soria R., Hau G. K. T., Graham A. W., Kong A. K. H., Kuin N. P. M., Li I. H., Liu J.-F., Wu K., 2010, *MNRAS*, **405**, 870
- Spera M., Mapelli M., 2017, *MNRAS*, **470**, 4739
- Steinhardt C. L., Elvis M., 2010, *MNRAS*, **402**, 2637
- Stone N. C., K pper A. H. W., Ostriker J. P., 2017, *MNRAS*, **467**, 4180
- Takekawa S., Oka T., Iwata Y., Tsujimoto S., Nomura M., 2020, *ApJ*, **890**, 167
- Terrazas B. A., Bell E. F., Henriques B. M. B., White S. D. M., Cattaneo A., Woo J., 2016, *ApJ*, **830**, L12
- Thompson T. A., et al., 2019, *Science*, **366**, 637
- Timlin John D. I., Brandt W. N., Zhu S., Liu H., Luo B., Ni Q., 2020, *MNRAS*, **498**, 4033
- Tolman R. C., 1939, *Physical Review*, **55**, 364
- Tully R. B., 1988, Nearby galaxies catalog. Cambridge: University Press
- Vall e J. P., 2019, *MNRAS*, **489**, 2819
- Vall e J. P., 2020, *New Astron.*, **76**, 101337
- Vogelsberger M., et al., 2014, *MNRAS*, **444**, 1518
- Volonteri M., 2012, *Science*, **337**, 544
- Volonteri M., Bellovary J., 2012, *Reports on Progress in Physics*, **75**, 124901
- Volonteri M., Rees M. J., 2005, *ApJ*, **633**, 624
- Volonteri M., Silk J., Dubus G., 2015, *ApJ*, **804**, 148

- Wajima K., et al., 2016, in Qain L., Li D., eds, *Astronomical Society of the Pacific Conference Series Vol. 502, Frontiers in Radio Astronomy and FAST Early Sciences Symposium 2015*. p. 81 ([arXiv:1512.03550](https://arxiv.org/abs/1512.03550))
- Weisskopf M. C., Tananbaum H. D., Van Speybroeck L. P., O'Dell S. L., 2000, *Chandra X-ray Observatory (CXO): overview*. SPIE, pp 2–16, doi:10.1117/12.391545
- Weisstein E., 2002, *CRC Concise Encyclopedia of Mathematics*. CRC Press, [https://books.google.com.au/books?id=D\\_XKBQAAQBAJ](https://books.google.com.au/books?id=D_XKBQAAQBAJ)
- Woo J.-H., Urry C. M., 2002, *ApJ*, 579, 530
- Woo J.-H., Cho H., Gallo E., Hodges-Kluck E., Le H. A. N., Shin J., Son D., Horst J. C., 2019, *Nature Astronomy*, 3, 755
- Wosley S. E., 2017, *ApJ*, 836, 244
- Wright E. L., 2006, *PASP*, 118, 1711
- Yang J., et al., 2020, *ApJ*, 897, L14
- Yoon I., 2017, *MNRAS*, 466, 1987
- Yu S.-Y., Ho L. C., 2018, *ApJ*, 869, 29
- Zackay B., Dai L., Venumadhav T., Roulet J., Zaldarriaga M., 2019, arXiv e-prints, p. [arXiv:1910.09528](https://arxiv.org/abs/1910.09528)
- Zasov A. V., Cherepashchuk A. M., 2013, *Astronomy Reports*, 57, 797
- Zaw I., Rosenthal M. J., Katkov I. Y., Gelfand J. D., Chen Y.-P., Greenhill L. J., Brisken W., Noori H. A., 2020, *ApJ*, 897, 111
- de Vaucouleurs G., de Vaucouleurs A., Corwin Herold G. J., Buta R. J., Paturel G., Fouque P., 1991, *Third Reference Catalogue of Bright Galaxies*. Springer, New York
- den Brok M., et al., 2015, *ApJ*, 809, 101
- van den Bosch R. C. E., 2016, *ApJ*, 831, 134
- von der Pahlen E., 1911, *Astronomische Nachrichten*, 188, 249